THESIS FOR THE DEGREE OF DOCTOR OF PHILOSOPHY IN MACHINE AND VEHICLE SYSTEMS

# Engine Encapsulation for Increased Fuel Efficiency of Road Vehicles

BLAGO MINOVSKI

Department of Mechanics and Maritime Sciences
CHALMERS UNIVERSITY OF TECHNOLOGY

Göteborg, Sweden 2017

Engine Encapsulation for Increased Fuel Efficiency of Road Vehicles
BLAGO MINOVSKI
ISBN 978-91-7597-636-5



Doktorsavhandlingar vid Chalmers tekniska högskola
Ny serie nr. 4317
ISSN 0346-718X
Department of Mechanics and Maritime Sciences
Chalmers University of Technology
SE-412 96 Göteborg
Sweden
Telephone: +46 (0)31-772 1000

Chalmers Reproservice
Göteborg, Sweden 2017

Engine Encapsulation for Increased Fuel Efficiency of Road Vehicles
Thesis for the degree of Doctor of Philosophy in Machine and Vehicle Systems
BLAGO MINOVSKI
Department of Mechanics and Maritime Sciences
Chalmers University of Technology

# Abstract

Thermal engine encapsulation is an increasingly popular design choice, which insulates the engine from the external environment and retains heat in the engine after it is turned off. This decelerates motor cool-down and increases the probability for high initial temperature at a subsequent engine start, resulting in shorter warm-up and reduced friction between engine parts.

This work investigates thermal engine encapsulation (TEE) as a means to reduce engine friction and fuel consumption during engine warm-up. In order to predict the effects of TEE on the fuel consumption, it is necessary to model a wide range of thermal phenomena in different subsystems of the powertrain. The presented work proposes an integrated simulation methodology that enables efficient numerical simulations of heat transfer in the powertrain cooling systems and the engine structures not only during dynamic driving but also during the process of engine cool-down when the vehicle is parked. The integrated simulation includes a number sub-models that capture relevant phenomena in the vehicle powertrain and underhood. Presented in detail is the simulation procedure, which ultimately predicts the continuous development of the temperatures of the engine oil and the coolant as well as the temperatures of the different engine parts and components from the powertrain cooling system. An automated coupling between the one-dimensional (1D) thermal representation of the engine and powertrain cooling systems with a three-dimensional (3D) CFD model of buoyancy-driven flow in the engine bay computes the heat rejection during engine cool-down. By use of an integrated friction correction map the engine model computes the variation of friction losses at different engine temperatures. The integrated simulation model makes possible to predict the temperature of engine structures after a long period of engine inactivity preceded by dynamic driving, the exact temperature development of engine structures and cooling fluids after a recurring engine start, as well as the variations in the instantaneous fuel consumption.

Furthermore, a TEE concept for a passenger vehicle has been designed. The presented simulation method is applied to evaluate the effect of the proposed encapsulation on the development of engine temperatures during cool-down and their effect on the fuel consumption during a sequence of two Worldwide harmonized light vehicle test cycles (WLTC) separated with a period of inactivity. The results indicate a significant capability of the encapsulation with high degree of coverage to retain engine heat for long time periods after key-off. This heat retention increases the probability for a warm subsequent engine start, which leads to a reduction in engine friction during engine warm-up. The obtained results show that the encapsulated engine setup has potential for up to 3.1% savings of the fuel burned during a WLTC by a non-encapsulated engine in a cold environment. The amount of fuel saved depends primarily on the specific engine (mass,

size and geometry), encapsulation design (geometry, thickness and degree of coverage), ambient temperature, and time of inactivity between engine shut-down and start-up. For periods of inactivity between 2 to 8 hours the potential for fuel saving is at least 2.5% of the total fuel burned during WLTC at an ambient temperature of $5°C$ for encapsulation with 97% coverage.

Keywords: thermal engine encapsulation, powertain cooling systems, cool-down, warm-up, numerical analysis, 1D simulations, 3D CFD simulations, coupled simulations, fuel consumption

# Acknowledgements

I would like to express my sincere gratitude to those, who made this work possible and who helped me during my studies.

First of all, I would like to thank my supervisors Ph.D Peter Gullberg and Professor Lennart Löfdahl for guiding and supporting me through all stages of my work, securing necessary connections and resources within the organizations, for their trust and vision. Furthermore, I would also like to acknowledge with much appreciation the manager of Simulation & Testing group and official manager of this project Peter Nilsson, who ensured a good environment for my work.
I would like to thank Ph.D Jelena Andrić for her constant support, invaluable cooperation and attention to detail. In addition I would like to thank all specialists at Volvo Trucks, who supported this project: Torbjörn Wiklund and Sassan Etemad for their help with the CFD simulations.
This project would not be possible without the funding provided by the Swedish Energy Agency within the framework *Strategic Vehicle Research and Innovation*.

Last, but not least I would like to thank all members of this project's Steering Committee for their conscious attitude and useful advice: Lennart Löfdahl, Peter Nilsson, Kjell Andersson from Volvo GTT, Alexander Broniewicz, Jerry Sjösten, Mats Löfman from Volvo Car Corporation and Per Jonsson and Mattias Chevalier from Scania.

# Nomenclature

| | | |
|---|---|---|
| $\sigma$ | Stefan-Boltzmann constant | $\left[\frac{W}{m^2K^4}\right]$ |
| $\varepsilon$ | Emissivity | $[-]$ |
| $\rho$ | Density | $\left[\frac{kg}{m^3}\right]$ |
| $\mu$ | Dynamic viscosity | $\left[\frac{kg}{sm}\right]$ |
| $A$ | Flow area | $\left[m^2\right]$ |
| $A_s$ | Heat transfer surface area | $\left[m^2\right]$ |
| $C_f$ | Skin friction coefficient | $[-]$ |
| $H$ | Total enthalpy | $\left[\frac{J}{kg}\right]$ |
| $K_p$ | Pressure loss coefficient | $[-]$ |
| $P_b$ | Brake power | $[W]$ |
| $R$ | Ideal gas constant | $\left[\frac{J}{kgK}\right]$ |
| $U$ | Velocity | $\left[\frac{m}{s}\right]$ |
| $V$ | Volume | $\left[m^3\right]$ |
| $e$ | Total internal energy | $\left[\frac{J}{kg}\right]$ |
| $h$ | Convective heat transfer coefficient | $\left[\frac{W}{m^2K}\right]$ |
| $k$ | Thermal conductivity | $\left[\frac{W}{m^2K}\right]$ |
| $m$ | Mass contained in a volume | $[kg]$ |
| $p$ | Pressure | $[Pa]$ |
| $q$ | Heat flux | $\left[\frac{W}{m^2}\right]$ |
| $u$ | Internal energy | $\left[\frac{J}{kg}\right]$ |

# Abbreviations

| | |
|---|---|
| 1D | One-dimensional |
| 3D | Three-dimensional |
| CAC | Charge air cooler |
| CAD | Computer aided design |
| CFD | Computational fluid dynamics |
| DNS | Direct numeric simulations |
| ECU | Engine control unit |
| EMS | Engine management system |
| FMEP | Friction mean effective pressure |
| ICE | Internal combustion engine |
| IMEP | Indicated mean effective pressure |
| NEDC | New European drive cycle |
| RANS | Reynolds-averaged Navier-Stokes |
| RT | Real time |
| TEE | Thermal engine encapsulation |
| URANS | Unsteady Reynolds-averaged Navier-Stokes |
| WLTC | Worldwide harmonized light vehicles test cycles |

# Thesis

This thesis consists of an extended summary and the following appended papers:

**Paper A** Minovski, B. and Lofdahl, L., "Study of Software Integration for Transient Simulation of Future Cooling System for Heavy Truck Application," SAE Technical Paper 2014-01-0653, 2014, doi:10.4271/2014-01-0653.

**Paper B** Minovski, B., Lofdahl, L. and Gullberg, P., "Numerical Investigation of Natural Convection in a Simplified Engine Bay," SAE Technical Paper 2016-01-1683, 2016, doi:10.4271/2016-01-1683.

**Paper C** Minovski, B., Andric, J., Lofdahl, L. and Gullberg, P., "Direct Coupled 1D-3D Approach for Simulations of Buoyancy-driven Heat Transfer in a Simplified Engine Bay, " Submitted to Applied Thermal Engineering, 2017

**Paper D** Minovski, B., Andric, J., Lofdahl, L. and Gullberg, P., "A Numerical Investigation of Thermal Engine Encapsulation Concept for a Passenger Vehicle and its Effect on Fuel Consumption, " Submitted to Journal of Automobile Engineering, 2017

# Contents

# Part I
# Extended Summary

# 1 Introduction

This chapter contains the reasons and motivations for starting this project and explains its relevance. The project goals are also outlined.

## 1.1 Background

ICE-driven vehicles continue to comprise the vast majority in today's means for ground transportation despite the recent advent of hybridization and electrification. The ubiquity of reciprocating combustion engines in modern transportation is expected to prevail for some decades to come mainly due to the maturity and convenience of the technology, the existing massive infrastructure that supports it, and last but not least, for economic reasons. However, ICE propulsion is heavily dependent on fossil fuel sources and has a negative impact on the environment. These challenges set the stage for the development and implementation of other methods for on-board energy conversion. They are also the main reasons that motivate the continuous improvement of ICE technology making it cheaper and cleaner than ever before.

The potential danger that an uncontrolled fossil-driven transportation poses to the climate and environment made governments enforce emission legislation to motivate carmakers to invest in advanced technologies that would allow for more efficient and cleaner propulsion. Figure 1.1 shows the requirements imposed by different countries on automotive producers. Obvious is a significant continuous reduction of the fleet-average limits for $CO_2$ emissions. The most ambitious target is 95 g/km of $CO_2$ emissions aimed by the European Union by 2021. A strict system requires manufacturers to pay a penalty of 95 € for every exceeded gram per km of $CO_2$ per vehicle sold. In response to this, automotive manufacturers continuously invest in research and development oriented to reduce fuel consumption and emissions. A great part of these efforts are focused on mitigating performance issues during cold-starts, which are mainly expressed as increased friction losses and emissions.

## 1.2 Improving vehicle efficiency by reducing friction losses in the powertrain

The increasingly tough emission targets and the competitive market set high performance requirements for the complete powertrain system. A major part of the total engine friction losses (45 to 80% [13]) originates from the oil-lubricated piston-crank and valvetrain assemblies, as shown in Figure 1.2. The friction in the piston-crank assembly increases with oil viscosity and therefore its portion of the total engine friction is even higher at

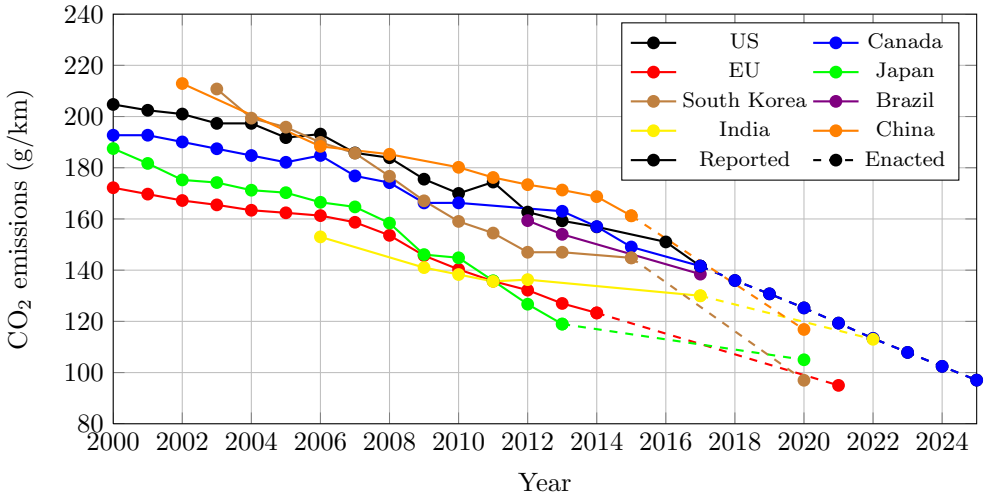


Figure 1.1: *Global $CO_2$ regulations for passenger cars in terms of NEDC g $CO_2$/km [10]*

low engine temperatures, i.e during engine warm-up. A study performed by Shayler et. al [34] investigated the effects of different oil viscosities on the additional load that a 2.4 l CI engine had to overcome due to the friction between its moving parts, defined as Friction mean effective pressure (FMEP). As a result of the increased lubricant viscosity in this experiment the engine's FMEP reached values approximately four times higher than in a fully warm engine. Therefore the additional friction losses that occur in an engine upon reaching operating temperature, i.e during warm-up, are significant and offer high potential for energy savings, especially in cold environments.

Different mechanisms for reducing cold-start engine friction losses have been explored and tested [31]. These methods are directed towards accelerating engine warm-up and prolonging engine cool-down. Some examples are hot-storage systems, preheating the engine oil and coolant with exhaust gases, coolant flow control, integrating phase change materials, and thermal insulation of the engine.

## 1.3 Working principle and characteristics of thermal engine encapsulation

By encapsulating different parts of the engine or the entire underhood compartment it is possible to reduce the magnitude of heat transfer between the engine and the ambient air. This slows down the cooling process after engine shut-off and increases the probability for high initial engine temperature at the following engine start, hence lowering the friction losses, which occur during a cold-start. Engine encapsulation is a viable engineering solution that addresses both thermal performance and acoustic design problems, utilizing the same infrastructure with a two-fold benefit. Furthermore, encapsulation designs which prevent unnecessary cooling air streams in some modes of operation from entering the

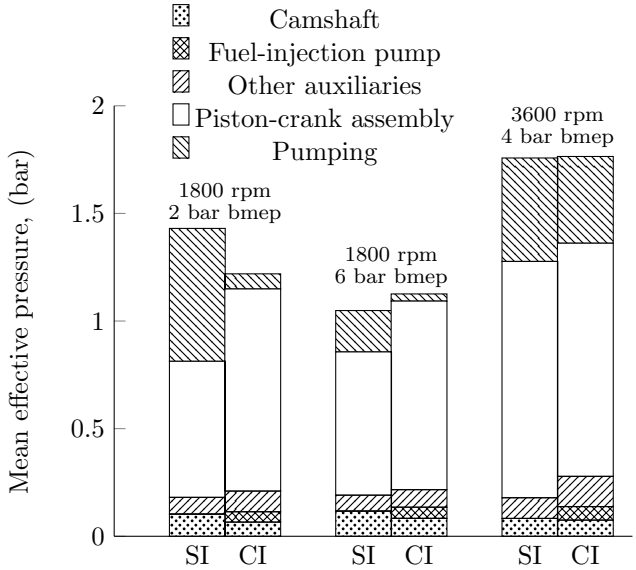


Figure 1.2: *Comparison of dominant types of friction losses for 1.6-liter four cylinder automotive spark-ignition (SI) and compression-ignition (CI) engines, Courtesy of Heywood [13].*

underhood reduce the overall aerodynamic drag of the vehicle. These designs usually utilize controllable air shutters or flaps, integrated closely downstream the grille, in order to allow for selective adjustment of the amount of cooling air flow. Such solutions, however, need to be carefully coordinated with the overall demands for engine cooling at multiple operating points to ensure that the engine encapsulation parts do not obstruct vehicle performance. Porous lightweight materials with low thermal conductivity and good noise absorption are used for the encapsulating structures.

Previously performed studies of the effects of thermal engine encapsulation delivered promising prognosis for the amount of the potential fuel savings and emission reductions. An experimental study, performed by one of the largest manufacturers of encapsulating materials, indicated that a fully encapsulated engine is capable of retaining its temperature above 40°C for up to 14 hours after shut-off in an ambient temperature of 20°C, while a non-encapsulated engine would cool down within 3 hours after key-off. Further analytical investigations, performed by the same authors, reported that for an annual mileage of 12300 km, thermal engine encapsulation can generate fuel savings of 5% in warm ambient and up to 9% in cold climates [32]. Similar results are reported by an experimental study performed by Mantovani et al. [22], who observed up to 2.7% reduction in $CO_2$ emissions. The authors of this study classified engine encapsulations in three main categories: engine-mounted, body-mounted and a combination of these. Engine-mounted encapsulation is located in close proximity to the engine structure, while body-mounted encapsulation encloses other components of the powertrain installation, including the cooling package. The study investigated the effectiveness of each encapsulation type from the perspective

of noise and $CO_2$ emission reductions. The results showed that most effective from thermal point of view is the combined engine-mounted and body-mounted encapsulation. An interesting observation reflected in this work is that the thermal effectiveness of encapsulation designs, manifested in their capability to retain engine heat over time, strongly depends on the area coverage of the encapsulation. The investigation reports that a 7 mm thick encapsulation covering 80% of the powertrain surface is equivalent to 50 mm thick encapsulation covering only 60%. The same study also addresses the acoustic benefits of the analyzed encapsulation types and indicates potential exterior noise reduction of up to 5 dB.

The above-mentioned works, however, provided little insight in the exact experimental and analytical methodology used to obtain the reported results. In this relation, Mattarelli et al. [5] presented a well-documented study of the effects of TEE for a small diesel engine. The authors draw conclusions about the effectiveness of the engine encapsulation with respect to the resultant cool-down time for different thicknesses of the insulation material. Furthermore, they proposed a simplified viscosity dependent model of engine friction, integrated with a 1D engine model, and validated using experimental measurements. The thermal engine model was combined with a simplified 0D model of heat transfer through the engine encapsulation to obtain predictions for the temperature development of the engine oil after shutdown. The presented methodology was employed to estimate the fuel savings resulting from the increased initial temperature at engine restart after 15 hours of inactivity at an ambient temperature of 0°C. The obtained fuel savings are reported to amount to 15% for the initial 15 minutes of a simulated drive cycle. Several other studies investigated similar aspects of TEE employing analogous methodologies: [27], [38], [36]. These studies reached to similar conclusions regarding the benefits of TEE with respect to $CO_2$ emissions and fuel consumption. Some of the previously reported predictions for the effectiveness of TEE in terms of fuel savings and $CO_2$ emission reduction are extensively optimistic and significantly varied in magnitude: 15% [5], 5% [32], 2.7% [22]. The variation of these estimations is partly explained by the different assumptions and boundary conditions used in each of these analyses. Furthermore, different authors use various coverage of engine encapsulation ranging from 60% [22] to close to 100% [5]. Clearly, an encapsulation which encloses 100% of the engine surface would provide excellent thermal insulation, but such installation would also be unfeasible in a real vehicle due to packaging and thermal constraints. In a general perspective most of the studies done on engine encapsulation employ oversimplified modeling strategies to estimate the effects of the buoyancy-driven heat transfer that takes place in the engine compartment after key-off. Sweetman et al. [37], on the other hand, presents a more advanced numerical method to capture the transient thermal soak phase after engine shutdown. Their method employs a 3D finite volume representation of the complete underhood, where buoyancy-driven flow is modeled by URANS and heat transfer is calculated in both solid and fluid domains. A satisfactory correlation is reached between computed and experimentally measured transient development of temperatures of air and solids during the soaking phase, but the employed numerical procedure requires significantly high computational resources (approx. 3800 CPU-hours to simulate 10 minutes of the soaking phase).

Central in the current work is an efficient numerical procedure for computing buoyancy-driven heat transfer in the engine bay to predict the temperatures of the engine oil and

the engine structures during driving sequences separated with extended periods of engine inactivity. The simulation method is applied to analyze the effects of a proposed engine encapsulation concept designed for Volvo S80 passenger vehicle on the engine cool-down and fuel consumption during warm-up.

Due to its multiple benefits, thermal engine encapsulation is an increasingly popular design choice in modern automotive industry. From a technical point of view there is a need to capture the effect of engine encapsulation on a system-level at an early stage of development, where the overall energy consumption of the vehicle is in focus. This work attempts to study the effects of thermal engine encapsulation in the context of the overall energy efficiency on a complete-vehicle level, while simultaneously capturing important underlying physical phenomena with sufficient depth.

## 1.4 Powertrain cooling and thermal management

Heat from combustion is conducted through the walls of the combustion chamber and exhaust ports into the block, head, valvetrain, pistons, crankshaft assembly, etc. Unless absorbed by another medium these heat fluxes would increase the temperature of engine components to detrimental levels. Powertrain cooling systems absorb the heat from the engine components and control their operating temperature within safe limits. In a typical engine installation cooling is performed by the oil and the coolant systems which usually conduct approximately 17 to 35 % of the heat released by the fuel, depending on the engine design and the specific mode of operation. For a control volume which surrounds the engine Heywood [13] provides an example of a mathematical representation of steady-state energy balance, Equation 1.1:

$$P_b + \dot{Q}_{cool} + \dot{Q}_{misc} + \dot{H}_{e,ic} + \dot{m}h_{e,s} = \dot{m}_f Q_{LHV}, \tag{1.1}$$

where $P_b$ is the brake power, $\dot{Q}_{cool}$ is the heat transfer rate to the coolant, $\dot{Q}_{misc}$ is the rate of heat rejection to the oil plus convection and radiation from the engine's external surface, $\dot{H}_{e,ic}$ is the exhaust enthalpy loss due to incomplete combustion, and $h_{e,s}$ is the sensible part of the specific enthalpy of the exhaust gases. The terms on the left-hand side of the equation represent the sinks and the single term on the right-hand side is the source - the rate of heat released by the fuel.

The unused heat from combustion travels through complex intertwining paths inside the engine. To map, quantify and control these heat flows is a main topic in engine thermal management. Engine encapsulation influences the heat flow in the engine by reducing the heat transfer from the engine walls to the surrounding environment. This affects the thermal balance of the engine and it is therefore important to understand and model it in the context of the overall engine thermal management. Furthermore, the temperatures of different engine components and fluids vary dynamically as a result of any momentary unbalance between the source and the sink. This happens often during regular driving, f.ex. during engine warm-up, when the source heat is bigger than the sink, as the radiator is bypassed, or during cool-down when the source heat is suddenly interrupted.

## 1.5 Analysis of powertrain cooling systems and thermal phenomena in the engine bay

### 1.5.1 Experimental analysis

Despite the progressively available and accurate numerical methods for virtual testing and analysis, experimental investigations continue to be an irreplaceable verification method in modern vehicle development. In order to ascertain that a cooling system design meets the overall performance requirements, various temperature and flow measurements in the powertrain cooling systems are simultaneously conducted during on-road or rig tests. Most effectively such tests are performed in specialized climatic windtunnels, where the ambient conditions are accurately controlled during test execution and the road load is replicated by a dynamometer roller system, coupled to the driving wheels of the vehicle. Figure 1.3 shows a heavy commercial vehicle prepared for a thermal performance test in a climatic wind tunnel.

Figure 1.3: *A commercial vehicle prepared for thermal performance testing in a climatic wind tunnel.*

### 1.5.2 Numerical analysis

In the context of thermal engine encapsulation and in order to predict its effectiveness it is crucial to obtain an accurate prediction for the initial engine temperature at engine shutdown, as it determines the initial heat content in the encapsulation upon the beginning of the cool-down process. Furthermore, the continuous development of engine temperatures during warm-up is also important for the evaluation of engine friction. This necessitates a suitable simulation model, which can predict the temperature variation of the engine structures and fluids in the powertrain cooling systems during vehicle operation. Such models include the complete powertrain cooling systems in combination with a thermal representation of the engine structures and a mechanical representation of the vehicle with road load input. Therefore they are implemented on a system level employing one-dimensional analysis. They are relatively fast and are therefore used for transient

analysis of long drive-cycles [Paper A], [21]. However, they require calibration, as inherent in their one-dimensional nature is the inability to provide detailed physical representation for some phenomena (turbulence, f.ex).

Another family of CFD models capture flow in three dimensions and operate with higher resolution, which allows for a more authentic representation of turbulent flow and heat transfer. In the past these models have been extensively used on smaller scale, f.ex on component level due to their high computational demand. However, with increasing availability of fast computing resources it has become industrially feasible to utilize such 3D CFD models on complete vehicle scales for steady flow and heat-transfer simulations, but also for short unsteady computations. Detailed three-dimensional numerical CFD representations of thermal and flow phenomena in a complete vehicle, including the engine structures, require sensitively large computational resources. This demand is increased even further when time is added as an extra dimension in the analysis [37]. Considering the time duration of interest in the context of thermal engine encapsulation, which amounts to cool down cycles of up to 16 hours, the computational demand for such analyses is an important constraint.

This work builds further on the current state of the art for numerical modeling of vehicle thermal management and attempts to deliver an automated procedure which allows feasible computations of the effects of thermal engine encapsulation designs on the fuel efficiency of the vehicle through a combination of 1D and 3D numerical tools.

## 1.6 Project objectives

The overall objective of this project is to enrich the knowledge within thermal engine encapsulation as a design choice with a focus on fuel efficiency. The general goal is subdivided into specific research questions:

- How does engine encapsulation influence fuel consumption?
- How can the effects of thermal engine encapsulation be estimated using numerical simulations and what are important factors to consider?

## 1.7 Outline of thesis

The first part of this work summarizes a number of experimental and numerical studies on the following topics:

- Transient energy transfer in powertrain cooling systems - methods, models and validation.
- Heat transfer in the engine bay.
- A computational procedure for numerical simulation of engine cool-down.
- Investigation of the effect of a proposed engine encapsulation on the fuel consumption.

The second part of this work contains four relevant articles produced during the course of the work.

# 2 Method

The work summarizes a sequence of coordinated studies on different technical aspects related to the effects of engine encapsulation on the continuous variations of engine temperatures and fuel efficiency. The presented work comprises both experimental and numerical investigations. All numerical models and procedures have been validated with corresponding experimental measurements. Included are stand-alone models of the powertrain cooling systems, as well as combined representations of the complete vehicle with heat transfer during the cool-down phase. A method for fast computation of engine cool-down is introduced. Furthermore, a thermal encapsulation concept for a passenger vehicle is presented and analyzed with the proposed integrated simulation approach.

## 2.1 Models of powertrain cooling systems with a drive-cycle input

### 2.1.1 Motivation

Ongoing efforts for engine downsizing have naturally affected the design requirements for all engine support installations including the powertrain cooling systems. Modern engine control units are programmed with a control strategy which monitors engine temperature and would derate engine power in the event of cooling deficiency. Clearly, engine cooling is crucial for vehicle performance and even though any eventual lack of cooling capacity would rarely result in a permanent engine failure it will certainly affect the overall vehicle performance and customer satisfaction. Therefore, the benefits from downsizing the cooling system must be carefully coordinated with the risks from an inevitable reduction in performance. Generally this has been done in a variety of field tests, but also analytically, especially in the early design phase. In this relation there is a need for a better understanding of the thermal interaction between the engine and the powertrain cooling systems not only for insulated steady-state modes of driving, but also for complete drivecycles. Such unsteady analysis of energy transport through the powertrain cooling systems can deliver information for the exact variation of the coolant and the oil temperatures in different parts of the respective system. Additionally, an unsteady representation of the powertrain cooling systems is of high value for the development of engine control systems. In the context of thermal engine encapsulation analysis it is crucial to be able to predict the continuous development of engine temperatures during a drive-cycle. This necessitates a transient thermal model of the engine coupled with the powertrain cooling systems, which can operate with a continuous input from a drive-cycle. A drive-cycle defines a speed requirement for the vehicle, which varies over time. A model is needed to transform this speed requirement into instantaneous heat conducted to the walls of the combustion chamber. This is done by a simplified dynamic representation of the vehicle, coupled with an engine model.

### 2.1.2 Longitudinal vehicle dynamics

The general modeling approach for the vehicle's longitudinal dynamics is guided by the fact that ultimately mechanical engine power affects vehicle speed through a dynamic system including the combined inertia of the powertrain, the mass of the vehicle and the resistance forces acting on the vehicle. Mathematically this is represented by Equation 2.1:

$$P_e \eta_{tr} = \dot{x}(1 + t_s)\left[\gamma_m m\ddot{x} + mg(f_r cos\alpha + sin\alpha) + \frac{1}{2}\rho C_d A\dot{x}^2\right], \tag{2.1}$$

where:

$P_e$ engine mechanical power

$\eta_{tr}$ driveline efficiency

$\dot{x}$ road speed

$\gamma_m$ coefficient of inertia of the rotating components

$m$ total vehicle mass

$\ddot{x}$ vehicle acceleration

$g$ gravitational acceleration

$f_r$ coefficient of rolling resistance

$\alpha$ road gradient

$\rho$ density of air

$C_d$ coefficient of aerodynamic drag

$A$ frontal projected area

$t_s$ tyre slip at driving wheels

With this relation, combined with information about the wheel rolling radius, one can obtain the instantaneous torque and speed that the engine must deliver in order to satisfy a certain road speed requirement from the analyzed drive-cycle for a given transmission gear. In this relation the wheel rolling radius would be used to convert the road speed to angular velocity of the wheels.

The longitudinal vehicle dynamic representation is combined with an engine model in order to deliver information about the instantaneous fuel consumption and heat rejected to the walls of the combustion chamber for a given road load. Modern one-dimensional tools for vehicle system analysis incorporate this methodology. More information on this topic is available in [Paper A] and [Paper D].

### 2.1.3 Physical setup of a simplified liquid-cooled powertrain cooling system

A simplified layout of a typical automotive cooling system is given in Figure 2.1. The

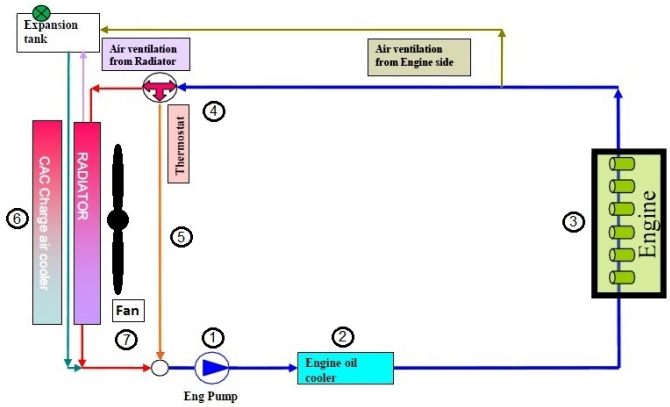


Figure 2.1: *A simplified layout of a powertrain cooling system.*

coolant pump ① drives coolant through the engine oil cooler ② and engine ③, where it absorbs heat. The bulk of the coolant stream continues towards a thermostatic valve ④, where it is passed on to the radiator in the cooling package ⑥, or in case of cold conditions it is diverted through a bypass line ⑤ back to the pump. The cooling air fan ⑦ ensures sufficient cooling air capacity at low vehicle speeds. The cooling fan and pump are the only components which require mechanical energy input and therefore affect fuel consumption. Hence, their control is an important task. In most automotive applications the coolant pump is mechanically coupled to the flywheel, while the fan is most often electrically driven in passenger vehicles. Since in commercial vehicles the fan is a significant energy consumer, it is coupled to the flywheel through a viscous or other type of clutch, see [Paper A] for further details. A condenser radiator, charge-air cooler and a radiator are stacked in a cooling package typically mounted in the front of the vehicle, where they are exposed to the incoming air stream, also referred to as ram-air. Other heat exchangers may be present depending on the specific vehicle configuration, f.ex: EGR-cooler, transmission oil cooler, air compressor cooler, cab heater, etc.

### 2.1.4 Modeling approach

One-dimensional (1D) system-oriented approach is usually an adequate choice to model the unsteady continuous operation of automotive powertrain cooling systems. The modeling framework considers a continuum where fluid motion is allowed only in the dominant stream-wise direction. Finite-volume approach is employed and the continuum is discretized in a staggered grid, that consists of a sequence of cells, where temperature and pressure are considered uniform. Vector quantities like velocity and heat flux are calculated at the boundaries of each cell. The fluid flow and energy transport in the

analyzed system are obtained through the solution of the Navier-Stokes equations in one dimension [12]. Equations 2.2-2.4, present the conservation equations for modeling fluid flow and energy:

$$\frac{dm}{dt} = \sum_{Boundaries} \dot{m} \tag{2.2}$$

$$\frac{d(me)}{dt} = -p\frac{dV}{dt} + \sum_{Boundaries} (\dot{m}H) - hA_s(T_f - T_w) \tag{2.3}$$

$$\frac{d\dot{m}}{dt} = \frac{dpA + \sum(\dot{m}u) - 4C_f \frac{\rho u|u|}{2} \frac{dxA}{D} - C_p\left(\frac{1}{2}\rho u|u|\right)A}{dx} \tag{2.4}$$

where:

$\dot{m}$ boundary mass flux into volume

$m$ mass of finite volume

$V$ volume

$p$ pressure

$\rho$ density

$A$ flow area

$A_s$ heat transfer surface area

$e$ total internal energy

$h$ heat transfer coefficient

$H$ total enthalpy

$T_f$ fluid temperature

$T_w$ wall temperature

$u$ velocity at boundary

$C_p$ pressure loss coefficient

$C_f$ skin friction coefficient

$dx$ length of mass element in the flow direction

$dp$ pressure differential acting across $dx$.

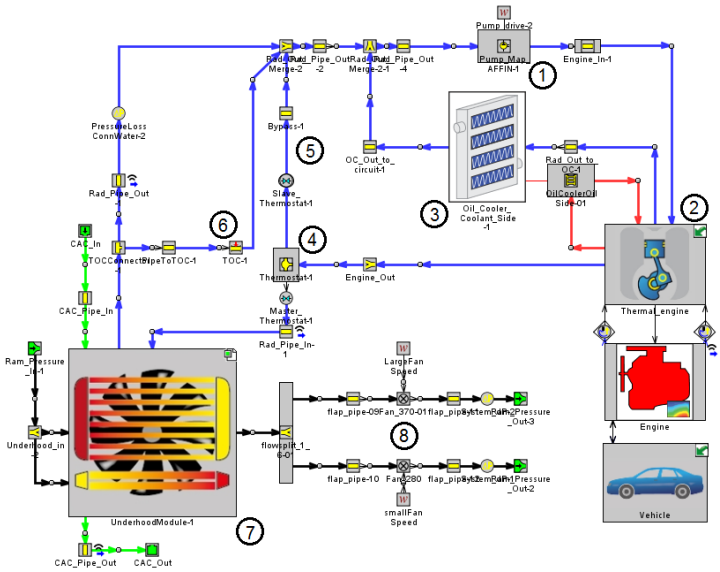


Figure 2.2: *Block diagram of a powertrain cooling systems model. Color legend: Coolant circuit, Engine oil, Charge-air, Cooling air.*

1D CFD tool GT-SUITE [12] has been used to model the powertrain cooling systems. A block diagram of the cooling system in a Volvo S80 is shown in Figure 2.2. The main layout is similar to the one shown in Figure 2.1 with only differences being that the oil cooler ③ is connected in parallel to the coolant pump ① and the presence of a transmission cooler ⑥. Each individual component of the cooling system is represented in the given model, including the heat exchangers, pumps, hoses, flow splits, thermostatic valve, coolant fan, etc. A 1D representation of these components is created. The pressure drops in hoses and other pipes are calculated using available empirical correlations and these usually do not require input of any additional data except for the pipe geometry. In order to calculate thermal performance of heat exchangers, however, it is necessary to supply the model with input performance data for the corresponding component. More information on 1D modeling methodology is available in [Paper A] and [12]. The dynamic representation of the vehicle, shown in the lower right corner in Figure 2.2, sends a signal for torque and speed demand to the engine map-based model connected above it. The engine performance representation calculates the amount of heat rejected to the walls of the combustion chamber and sends it to the thermal model of heat conduction in the engine structures ②. This model is important not only for correct transient prediction, but it also enables the calculation of the oil temperature as a result of the internal energy balance, obtained from the representation of heat transport in the engine structures. A block diagram of a thermal engine model is given in Figure 2.3. It consists of a cluster of interconnected lumped thermal masses, which represent sections from the physical engine structures - portions from the cylinder head, block, cylinder liners, etc. They are interconnected with thermal resistances, calibrated to authentically simulate

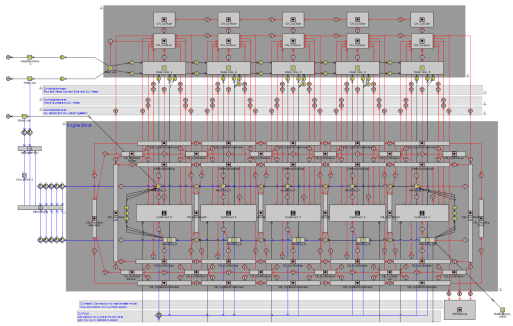

Figure 2.3: *Block diagram of a thermal engine representation. The heat transport through the engine structures is represented by a network of thermal masses.*

transport of heat in the engine block. The cooling channels inside the engine block are represented with flow volumes, which are also thermally interfaced with the adjacent lumped thermal masses. Heat conduction in one dimension is resolved in all solid masses as given in Equation 2.5.

$$Q = c_p \frac{\partial T}{\partial t} - k\left(\frac{\partial^2 T}{\partial X^2}\right). \tag{2.5}$$

Here $c_p$ represents the specific heat capacity, $T$ is the temperature, $t$ denotes the time, $Q$ is the source heat flux, $k$ is conductivity, and $X$ is the spatial dimension.

## 2.2 Validation of powertrain cooling system models

A large number of simulations were performed to ascertain the accuracy of the employed 1D cooling system models. Executed were simulations of continuous drive cycles for a distribution commercial vehicle and the computed results for different performance quantities were compared to rig measurements. Figure 2.4 presents a comparison between the simulated and the measured results for the radiator outlet temperature from a simulation of Hamburg-Kassel drivecycle for a 13-liter Volvo FH truck with an authentic fan control algorithm implemented in the cooling system model. Similar comparisons are available for other temperature readings and flow capacities calculated in the simulation, e.g.: charge air outlet temperature, coolant mass flow through the radiator, etc. More information about 1D cooling system model validation can be found in [Paper A] and [25].

## 2.3 Temperature dependent variations in engine friction

The ability to evaluate the variations in engine friction with the engine temperature is important because it is the retention of engine temperature which directly results in reduced friction losses. To be able to quantify any resulting fuel savings it is necessary

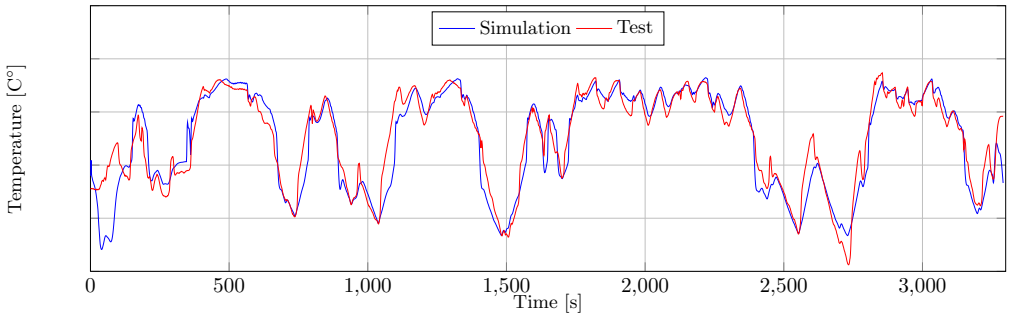


Figure 2.4: *Radiator outlet temperature. A comparison between measured and simulated values.*

to obtain a relation between the engine temperature and the variation of friction mean effective pressure (FMEP). Equation 2.6 proposed by Leong et al. [19], [40] characterizes engine friction as a function of oil viscosity:

$$FMEP = FMEP_{fully\ warm} \left( \frac{\mu}{\mu_{fully\ warm}} \right)^{n}, \tag{2.6}$$

where $\mu$ is the viscosity of the engine oil and the exponent $n$ is typically in the region of 0.19-0.24 for gasoline engines and 0.25-0.32 for diesel engines.

An improvement to the method presented in Equation 2.6 includes a product of FMEP at nominal engine temperature with an empirical coefficient dependent on the engine temperature and engine speed:

$$FMEP_{Corrected} = (1 + C_B) \times FMEP_{fully\ warm}, \tag{2.7}$$

where $C_B$ is a correction factor shown in Figure 2.5.

The presented approach to compute engine friction has been used in the analysis due to the fact that it has proved to be accurate and its implementation requires relatively little input data.

## 2.4 Model of buoyancy-driven heat transfer in the engine bay

### 2.4.1 General principles

The thermal phenomena which occur in the engine bay after engine shutdown in the absence of forced flow are defined as buoyancy-driven flow and resulting convective heat transfer and thermal radiation. In such combined scenarios where thermal radiation and natural convection are significant, it is important to provide numerical models, which capture both mechanisms of heat transfer. The local density variations in the fluid, caused

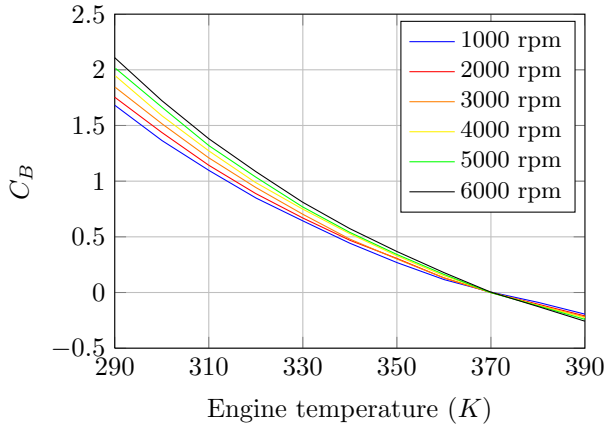


Figure 2.5: *Coefficient $C_B$ for correction of FMEP at different engine speeds.*

by the temperature gradients, result in buoyant forces, which induce momentum in the fluid, causing it to move. The intensity of buoyancy-driven flows is characterized with the ratio between the buoyant forces, which strive to move the fluid and the viscous forces, which are opposed to any movement. This ratio is known as the Grashof number and it is defined as following:

$$Gr_x = \frac{g\beta}{\nu^2}(T_s - T_\infty)x^3, \tag{2.8}$$

where $\beta$ is the coefficient of thermal expansion, $\nu$ is the kinematic viscosity, $T_s$ is the surface temperature, and $x$ is a characteristic length. In the context of numerical modeling, it is important to know the prevailing flow regime in the analyzed setup in order to make a relevant choice for modeling the flow. According to Bejan [3], the transition between laminar and turbulent flows occurs when the Grashof number is approximately 1.3 $\times 10^9$ for vertical plates. The local surface temperatures of the engine often reach values higher than 100°C. Substitution with numerical values from a typical scenario of thermal soak in Equation 2.8 gives results of approximately 1.9 $\times 10^9$, indicating that the flow has entered the transition regime, see Table 2.1. Hence, a suitable turbulence model would be required for the correct numerical representation of the analyzed flow phenomenon.

### 2.4.2 Modeling physics

To describe the complex dynamics of the fluid motion under the conditions of natural convection in the underhood a classical approach has been selected that involves the solution of the continuity equation 2.9, the transport equation for momentum 2.10, and the static enthalpy conservation equation 2.13.

$$\frac{\partial(\rho U_i)}{\partial x_i} = 0, \tag{2.9}$$

where $\rho$ is the density and $U_i$ is the mean velocity component in the $i$-th direction.

$$\frac{\partial(\rho U_i U_j)}{\partial x_i} = -\frac{\partial p}{\partial x_i} + \frac{\partial}{\partial x_j}(\tau_{ij} - \rho\overline{u_i' u_j'}) + \rho g_i. \tag{2.10}$$

Here $\tau_{ij}$ is the averaged viscous stress tensor, $p$ is the static pressure, and $\rho\overline{u_i' u_j'}$ represents the components of the Reynold's stress tensor, where $u_i'$ and $u_j'$ are the fluctuating turbulent velocities. The source term $\rho g_i$ takes into account the effect of buoyancy, where $g_i$ is the $i$-th component of the gravitational acceleration.

The average viscous stress tensor $\tau_{ij}$ reads

$$\tau_{ij} = \mu\left(\left(\frac{\partial U_i}{\partial x_j} + \frac{\partial U_j}{\partial x_i}\right) - \frac{2}{3}\frac{\partial U_k}{\partial x_k}\delta_{ij}\right), \tag{2.11}$$

where $\mu$ is the dynamic viscosity of the fluid and $\delta_{ij}$ are the Kronecker delta tensor components, *i.e.*

$$\delta_{ij} = \begin{cases} 0 & \text{if } i \neq j, \\ 1 & \text{if } i = j. \end{cases} \tag{2.12}$$

$$\frac{\partial}{\partial x_i}(\rho U_i H) = -\frac{\partial}{\partial x_i}(Q_i + \rho\overline{u_i' h'}), \tag{2.13}$$

The presented formulation is not time dependent and therefore its solution provides results for a steady flow field. In the context of buoyancy-driven flow in an engine bay it has been proven that for constant boundary conditions a steady solution of the Navier–Stokes equations delivers satisfactory predictions of the temperature and velocity fields in the fluid [8], [Paper B]. In the process of cool-down, however, boundary conditions do vary with time. To capture this variation and its effects on the flow-field, it would be natural to chose an unsteady formulation of the Navier-Stokes equations. Nevertheless, such solution is unfeasible for extended simulation periods on the scale of 16 hours, due to the need for high temporal resolutions in the solution of the flow field, which results in impractically long computational runtime. To address this problem a direct-coupled 1D-3D approach has been proposed and validated in [Paper C].

Table 2.1: Estimation of buoyancy-driven flow characteristics in a typical engine bay.

| Term | Quantity |
|---|---|
| g (m/s) | 9.81 |
| $\beta$ (1/T) | 0.00306 |
| $T_s$(C) | 100 |
| $T_\infty$(C) | 5 |
| $x$ | 0.5 |
| $\nu$ ($m^2$/s) | $1.807 \times 10^{-5}$ |
| $Gr_x$ | $1.9 \times 10^9$ |

**Solution of flow and heat transfer in the oil sump**

As a result from the transient engine cool-down after key-off the temperature of the oil sump wall decreases gradually over time, absorbing heat from the engine oil contained in it and conducting it away to the ambient. The process of heat rejection from the engine oil to the wall is accompanied with a density variation, which generates buoyancy-driven flow. Assuming an extreme temperature difference between the wall and the engine oil, $(T_s - T_\infty) = 15\text{K}$, for high oil temperatures, $T_\infty = 403\text{K}$ and characteristic length equal to the height of the oil level in the sump, $x = 0.075\text{m}$, the resulting Grashof number is $1.35 \times 10^6$. Therefore, the analyzed thermal-fluid phenomenon observed in the oil sump is characterized as natural convection in laminar flow. Furthermore, static adjacent layers with well-pronounced temperature difference are present, also referred to as temperature stratification. Evident in Figure 2.6 is a significant temperature gradient in proximity

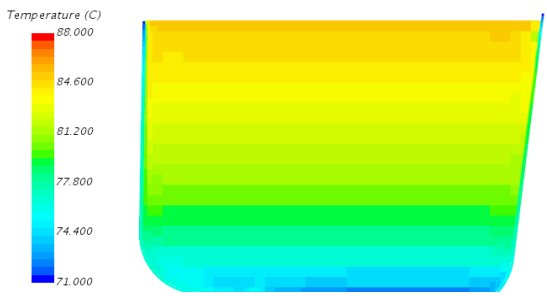


Figure 2.6: *Simulated temperature field in a longitudinal section cut of the oil sump extracted 1 hour after key-off in a non-encapsulated engine at the ambient temperature of* $25°C$

to the wall, which amounts to approx. 30% of the instantaneous temperature difference between the oil and the ambient air. This strong spatial variation of the oil temperature invalidates the usage of 1D tools for its appropriate prediction. On the other hand, the non-turbulent flow regime in the oil sump precludes the necessity for computationally expensive turbulence modeling, and allows to set up a fast-running three-dimensional transient analysis of buoyancy-driven laminar flow, which is directly synchronized with the 1D transient solution of the powertrain.

### 2.4.3 Computational grid and numerical domain

A full-scale CAD model of the simulated vehicle, placed in a large enclosure, is used to generate a computational mesh of approximately 60 million cells in StarCCM+. Figure 2.7 shows a section cut through the computational grid taken at the vertical longitudinal central plane in the region of the engine bay. Included are representations of the condenser radiator, CAC, and coolant radiator. The maximum cell size in the underhood area has been limited to 10 mm. Cells in proximity to the engine walls are limited to 3mm in size. A layer of prism cells at the wall boundaries ensured $y^+$ values of close to 1, as recommended by the simulation software manual [4] and confirmed by previous investigations [Paper C],

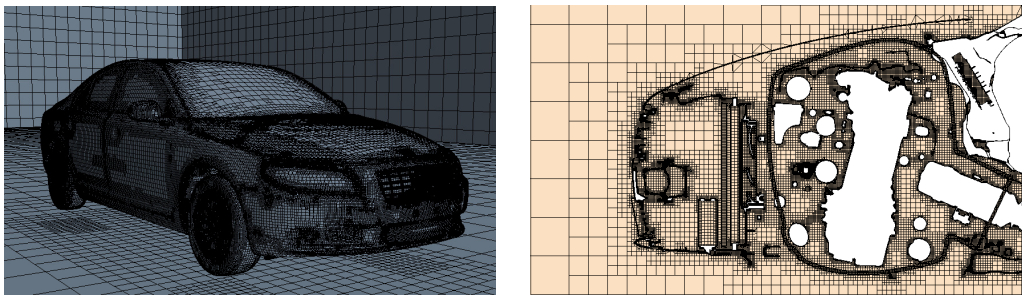

(a) *Discretized surface* (b) *Planar section through the grid*

Figure 2.7: *Computational grid.*

[8]. More information related to the numerical grid can be found in the attached articles.

### 2.4.4 Boundary conditions

All walls in the numerical setup are defined with a non-slip condition. Constant ambient temperature is imposed on the walls of the enclosing chamber. The main aim of the presented model is to obtain accurate values for instantaneous heat fluxes from the engine parts identified as major participants in convective and radiative heat transfer after key-off, due to their big relative mass, high thermal conductivity and large exposed surface area. These parts include the cylinder head, engine block, crankcase, gear box, exhaust manifold, exhaust pipe, and turbo-compressor. These components have their corresponding representations in the 1D engine thermal model, which supply information for surface temperature to their respective boundaries in the 3D CFD model, see Figure 2.8.

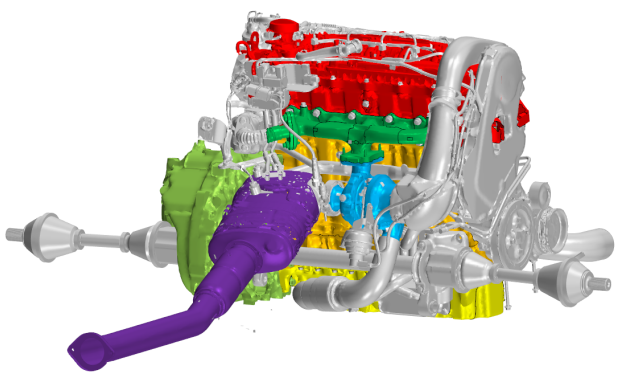

Figure 2.8: *3D CFD engine wall boundaries with imposed temperature specification coordinated with 1D engine thermal model. Color legend: Cylinder head, Engine block, Oil sump, Gear box, Exhaust manifold, Turbo-compressor, EATS and exhaust pipe.*

## 2.5 Automation and numerical strategy

The proposed numerical procedure for fast computation of buoyancy-driven heat transfer utilizes a sequence of steady state solutions of flow and energy transport in the fluid done in StarCCM+, synchronized with an unsteady solution of heat transfer in the solids executed in GT-SUITE. Exchanged between the different simulations are coefficients of heat transfer and information for surface temperature. The constructed simulation setup accommodates the possibility to run combined drive-cycles, which include periods when the vehicle is parked with the engine turned off. An automation routine that controls the execution of the different simulations and their coordination is developed in Java. A description of the actions performed by this software is given next.

The simulation is typically started with a stage of dynamic driving with variable demand for vehicle speed, which imposes an unsteady requirement for engine speed and torque and initiated from ambient temperature. During this stage when the engine is running the 1D representation of the engine and powertrain cooling systems run independently from the 3D CFD model. Calculated is the dynamic development of temperatures in solids and fluids in the cooling systems. Upon engine shutdown the surface temperatures of the solids in the 1D thermal engine representation are extracted and imposed as boundary conditions on the 3D representation of buoyancy-driven heat transfer in the engine bay. The 3D CFD simulation is then run until convergence and results for heat transfer coefficient from all participating surfaces are exported and imposed in the 1D thermal engine model, which is consequently run for a defined period before a new cycle of exchange between the softwares is completed. The process is described as a flowchart in Figure 2.9.

## 2.6 A proposed concept of thermal engine encapsulation for a passenger vehicle

An engine-mounted thermal engine encapsulation concept is proposed for the purposes of the investigation, see Figure 2.10. The presented design concept features two separate openings equipped with air shutters: one located on the front of the encapsulation, immediately behind the cooling fan, and another one - located near the exhaust routing. Such a setup is applicable in cases of high load driving when the air shutters can be opened in order to allow for additional cooling air flow to mitigate the undesirable effects of hot spots and to provide extra cooling in situations when this is needed. Closing the air shutters, on the other hand, would prevent ambient air from entering the encapsulation and consequently this would increase its capability to retain engine heat. In this manner the proposed design offers an effective solution to the most serious shortcomings of thermal engine encapsulation (hot spots and increased blockage in the underhood) by enabling a selective variation in the degree of encapsulation. The presented encapsulation concept is designed with a number of unsealed openings to allow passage for brackets, cooling hoses and drive-shafts. These openings are not sealed or insulated in order to explore a scenario of possible air leakage through the encapsulation. The ratio of the open surface area to the complete outer surface coverage of the encapsulation with closed shutters is

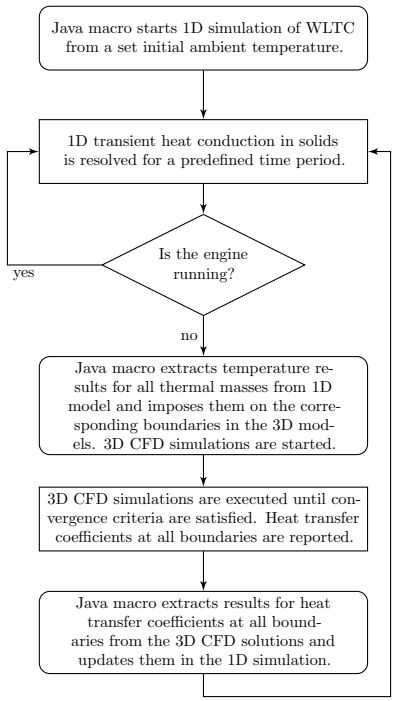


Figure 2.9: *Flow chart describing the coupling procedure between 1D and 3D models.*

97%. The outlet of the proposed design is shaped to channel the cooling air stream along the surfaces of the exhaust components in order to increase the rate of convective cooling during the initial stages of thermal soaking, while also providing radiation shielding. Its downwards orientation is selected to prevent buoyancy forces from transporting hot air outside the encapsulation when the shutter is open. A lightweight melamine resin with low thermal conductivity is selected for the encapsulating panels.

## 2.7 Drive-cycle simulations

To evaluate the effectiveness of the presented thermal engine encapsulation it is proposed to construct a dedicated drive-cycle, which consists of sequences of WLTC, separated with periods of inactivity, initialized from ambient temperature. This allows for a prediction of the initial temperature of engine solids in the beginning of the cool-down phase. Similarly, the computed temperatures of the engine components after the cool-down, that takes place in the period of engine inactivity, are used as initial conditions for the second WLTC. Computed values for fuel consumption are obtained during the analysis. Sequences of WLTC with periods of inactivity of 0.5, 1, 2, 4, 6, 8, 12, and 16 hours are used, as shown in Figure 2.11. In order to obtain knowledge about the effect of different ambient temperatures on the effectiveness of the encapsulation, simulations were performed at temperatures of 5 and 20°C, representing moderately cold and warm climate conditions

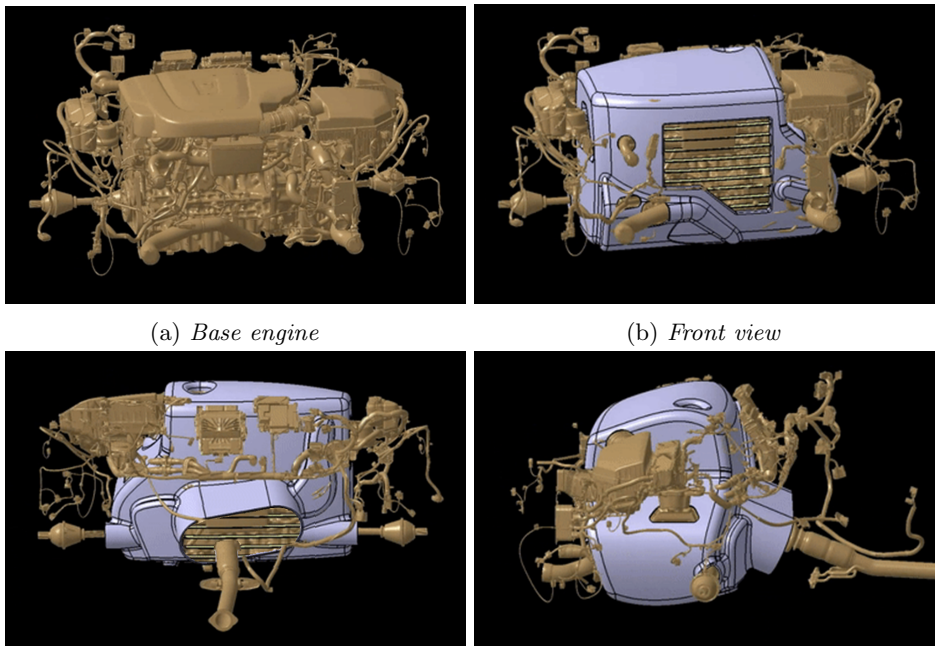

(a) *Base engine* (b) *Front view*

(c) *Back view* (d) *Side view*

Figure 2.10: *Thermal engine encapsulation concept.*

respectively.

Simulated are cases with closed and open shutters to observe the effect of the degree of engine encapsulation. The main performance parameters, monitored and reported during the analysis, are among others the temperatures of engine oil and the instantaneous and accumulated fuel consumption. Table 2.2 presents an overview of the simulated cases and their characteristics.

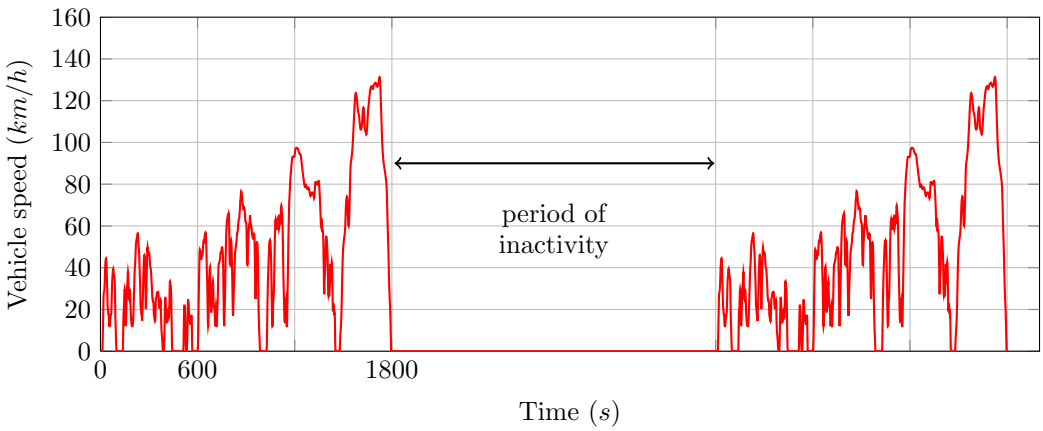


Figure 2.11: *Simulated drive-cycle consisting of sequences of WLTC with different periods of inactivity.*

Table 2.2: Overview of simulated combinations

| Ambient temperature $°C$ | Non-encapsulated | Encapsulated with open outlet shutter | Encapsulated with closed shutters |
|---|---|---|---|
| 5 | • | • | • |
| 20 | • | • | • |

• 0.5, 1, 2, 4, 6, 8, 12 and 16 hours of inactivity

# 3 Summary of results

This section contains a summary of the most important findings from the research work. More detailed information about the results can be found in the appended papers.

## 3.1 Simulations of transient cool-down of a simplified engine

This investigation is performed as an initial validation of the proposed computational strategy, which utilizes a direct coupling between a 1D representation of heat conduction in the engine structures and a 3D CFD model of buoyancy-driven flow and heat transfer in the engine bay. The measurements used for this investigation originate from an experimental study of natural convection in a simplified engine bay performed by Davis [9] and Merati *et al.* [23] that employs a simplified engine bay in full scale. It consists of a trapezoidal shaped engine, two exhaust cylinders with diameter of 45.7 mm and length of 0.56 m, identical in size mounted on the left and right sides of the engine block, and an enclosure with openings to the surrounding air with approximate size of 0.85 m in hight, 0.92 m width and 0.9 m in length, see Fig. 3.1. The enclosure has two 5 mm wide openings on the top side and two 153 mm wide openings in the bottom of the left and right sides. The two openings at the top represent the gaps between the vehicle hood and the fenders, while the side openings at the bottom facilitate the thermal interaction with the quiescent surrounding air to occur. Moreover, the complete setup was placed in a containment area with dimensions of 4.9 m in width and length and 3 m in height, which is sufficiently larger than the dimensions of the enclosure to avoid disturbances of the thermal and flow phenomena involved [9]. The exhaust manifolds, the simplified engine and the enclosure are relevant components of a typical vehicle underhood which mark the maximum temperature range that occurs during thermal soak. Therefore, this setup provides a suitable experimental ground for conducting a validation of the coupled computational method for predicting underhood buoyancy-driven flow and heat transfer.

The experiment replicates a thermal process governed by buoyancy-driven flow and heat transfer. The surface temperature of the exhaust manifolds was maintained at 600°C with inbuilt electrical heaters. Meanwhile the engine walls were cooled by internal water jet system, ensuring that the temperature of the engine is close to 100°C. It was determined that the heaters, mounted in the exhaust manifolds, dissipated approximately 2500 W of heat each, which corresponds to a heat flux of 31 kW/m$^2$. These conditions were maintained constant until readings from temperature sensors mounted on the walls of the simplified engine stabilized, indicating steady heat fluxes. At this situation of steady-state heat transfer, surface temperature measurements were obtained on all solids. The locations of the thermocouples, used for these measurements, are given in subsection 3.1.1. After performing the steady temperature measurements, all heat and cooling sources were shut down and transient cool-down was started. Surface temperatures of all solid parts in the setup were monitored for a period of 35 minutes after shutdown.

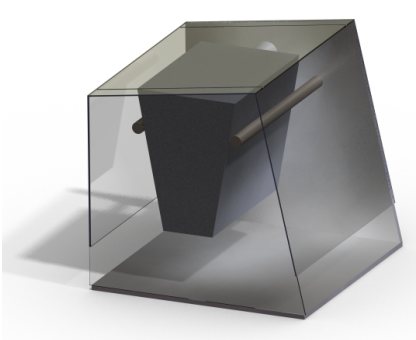

(a) *Representation of the experimental setup under enclosure.*

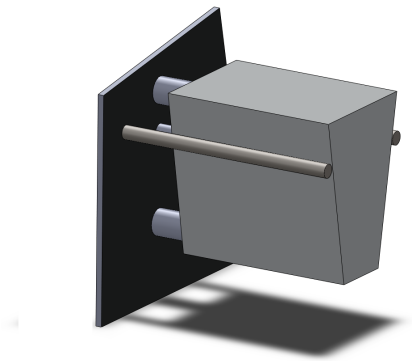

(b) *Simplified engine and exhaust manifolds.*

Figure 3.1: *A CAD model of the experimental setup comprising of the simplified engine and two exhaust manifolds under the open enclosure.*

### 3.1.1 Numerical setup

An exact CAD model of the engine bay, placed in the containment volume, see Fig.3.2, was built according to the presented experimental setup.

It is important to note that the domain consists of the solid and the fluid subdomains. The solid subdomain comprises the engine, the exhaust manifolds, and the enclosure. The fluid subdomain includes the air, which fills the volume under the enclosure, as well as the surrounding containment area. This concept of two separate subdomains makes it possible to employ the most suitable models for the fluid and solid parts, respectively, and to establish a direct coupling between these models.

Figure 3.3 presents schematics of the 1D thermal model of heat transfer in the engine solids. The simplified engine and the exhaust manifolds are represented by lumped thermal masses, as shown in Fig. 3.3a. The concept of lumped thermal masses is based on the assumption that the temperature differences within a solid, participating in heat transfer with a surrounding medium, can be neglected as compared to the temperature difference between the solid and the fluid. Previous experimental and numerical results have shown that this approach is valid for the exhaust manifolds and for all engine surfaces except the right and left engine walls, see Merati *et al.* [23] and Chen *et al.* [8] for more details. A good example of solids which can be accurately modeled using a single lumped thermal mass are the exhaust manifolds, for which experimental observations confirmed negligible internal temperature differences and uniform temperature distribution on their surfaces. The surfaces of the left and right engine walls, on the other hand, exhibit significant temperature gradients due to high radiative heat flux from the adjacent exhaust manifolds. Therefore, each of the engine side walls is represented by a network of 55 interfaced lumped thermal masses to provide sufficient spatial discretization to accurately capture the temperature distribution, see Fig. 3.3b. The specific topography and dimensions of the thermal masses comprising this network are chosen so that their centers coincide with the locations of the thermocouples from the experiment, as illustrated in Fig. 3.4. The

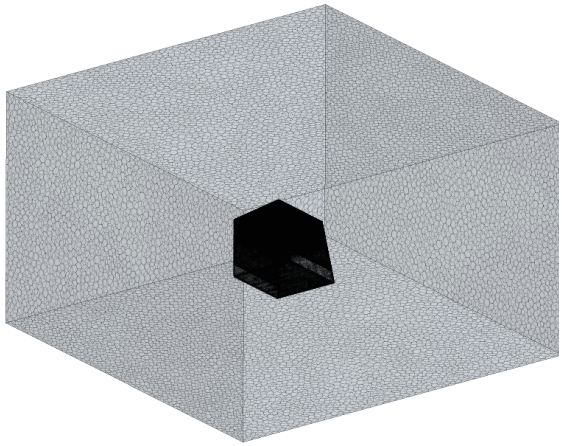

Figure 3.2: *Computational domain comprising the simplified engine and two exhaust manifolds under the open enclosure (black area) placed in the containment room (gray area).*

lumped thermal masses in the model are defined with the physical properties, dimensions and weights of the actual materials used to build the experimental engine. It should be noted that each row of interfaced thermal masses in the network representing the engine side wall corresponds to one row of adjacent sectors of the physical wall from top to bottom.

The governing equations of the fluid flow are numerically solved in STAR-CCM+. A polyhedral computational mesh with a total cell count of 25 million is generated from the CAD model of the enclosure and the containment area. The average spatial discretization varies within the limits of 2 and 120 mm depending on the location. Denser mesh is used in the vicinity of the exhaust manifolds and in the upper part of the enclosure to more accurately resolve the temperature gradients and the buoyancy-driven flow field. The maximum cell size is 3mm for all the surfaces located above the exhaust manifolds. The thickness of the first prismatic layer on the surfaces is approximately 0.3 mm, which results in maximum $y^+$ values of close to 1. The temperature development in the solid structures is consequently computed using the described 1D–3D coupled procedure.

### 3.1.2 Results

A coupled 1D–3D simulation is carried out to predict the temperature development in the engine solids during the thermal soak and cool-down period after turning off the heating and cooling systems. The coupled simulation is initiated from a fully developed solution of steady heat transfer. The data exchange between 1D and 3D computational domains takes place every 5 seconds. The coupled simulation predicts the temperature development in each thermal mass. Figure 3.5 presents the development of the average surface temperature of the engine walls and the exhaust manifolds during the cool-down

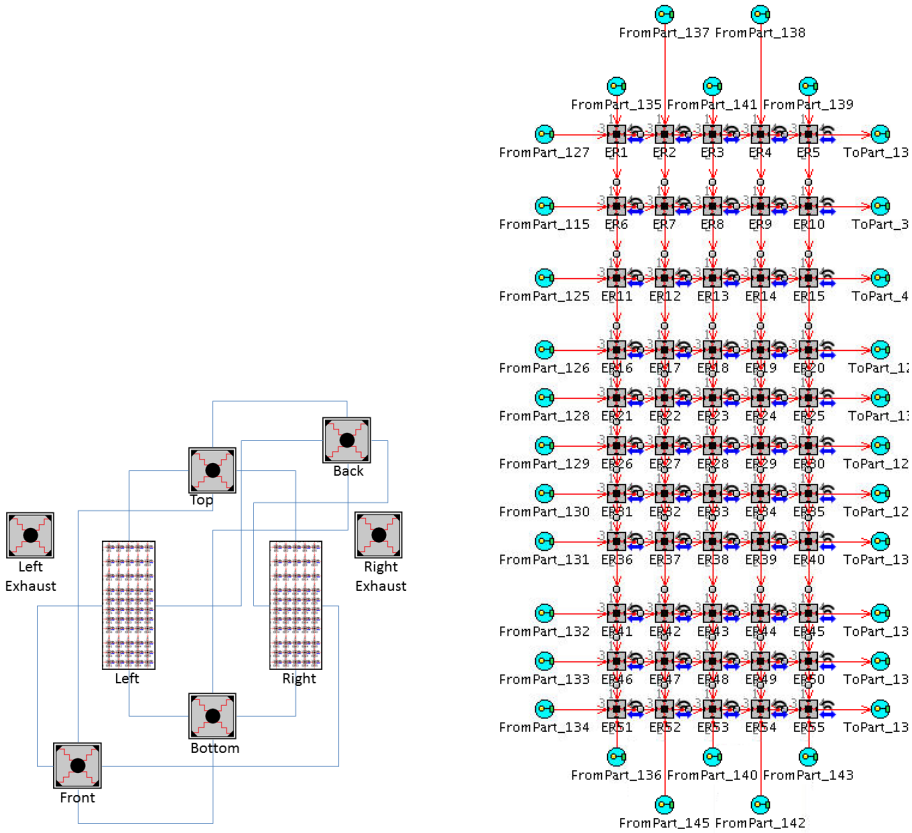


(a) *A block diagram of the 1D thermal model of heat conduction in the simplified engine.*

(b) *Network of thermal masses representing each of the side walls of the simplified engine.*

Figure 3.3: *Schematics of the 1D thermal model in GT-SUITE.*

cycle of 35 minutes. The results from the actual experimental study are included for the purpose of validation. A very good agreement between the computed and measured temperature results is seen for both exhaust manifolds and the right engine wall. The surface temperature of the left engine wall is underpredicted by approximately 3% as compared to the experimental results. This discrepancy is attributed to the fact that the simulations do not accurately account for the presence of the gaskets that are used to seal the adjacent metal plates that comprise the simplified engine.

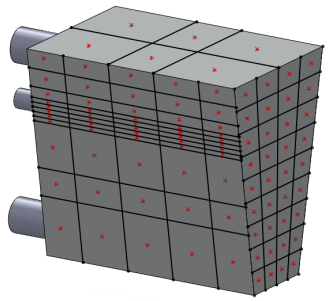

Figure 3.4: *The simplified engine with indicated locations of the thermocouples from the experiment.*

## 3.2 Simulation of transient engine cool-down in a passenger vehicle

The following investigation is undertaken in order to provide a further validation of the presented computational procedure for an experimental setup that involves the original geometry of a passenger vehicle. The current investigation utilizes data from thermal measurements obtained from complete vehicle dynamometer tests in a climatic wind tunnel for the purpose of correlation with simulated values and model validation. The drive cycles replicated in these measurements included steady-speed and high load driving, as well as dynamic driving with varying engine loads and speeds. The powertrain system was equipped with sensors to obtain various measurements: inlet and outlet temperatures of all heat exchangers, coolant and flow rates, fan speeds, and all signals to the ECU were logged. Most relevant for the analysis are the temperatures of the coolant and the engine oil during the transient process of engine warm-up and cool-down.

### 3.2.1 Numerical setup

Included in this simulation model are functional blocks which allow to replicate the instantaneous heat input from the engine during a continuous drive-cycle in addition to a complete 1D representation of the powertrain cooling systems, including the coolant and oil circuits, as described in chapter 2. The described coupled 1D–3D numerical strategy has been applied to obtain predictions for engine oil and coolant temperature development after key-off.

### 3.2.2 Results

The simulation models of the coolant circuit and the cooling air path were first calibrated to ensure correct prediction of the coolant flow and the cooling air flow mass rates at different vehicle and engine speeds. Figure 3.6 shows a comparison between the measured and the

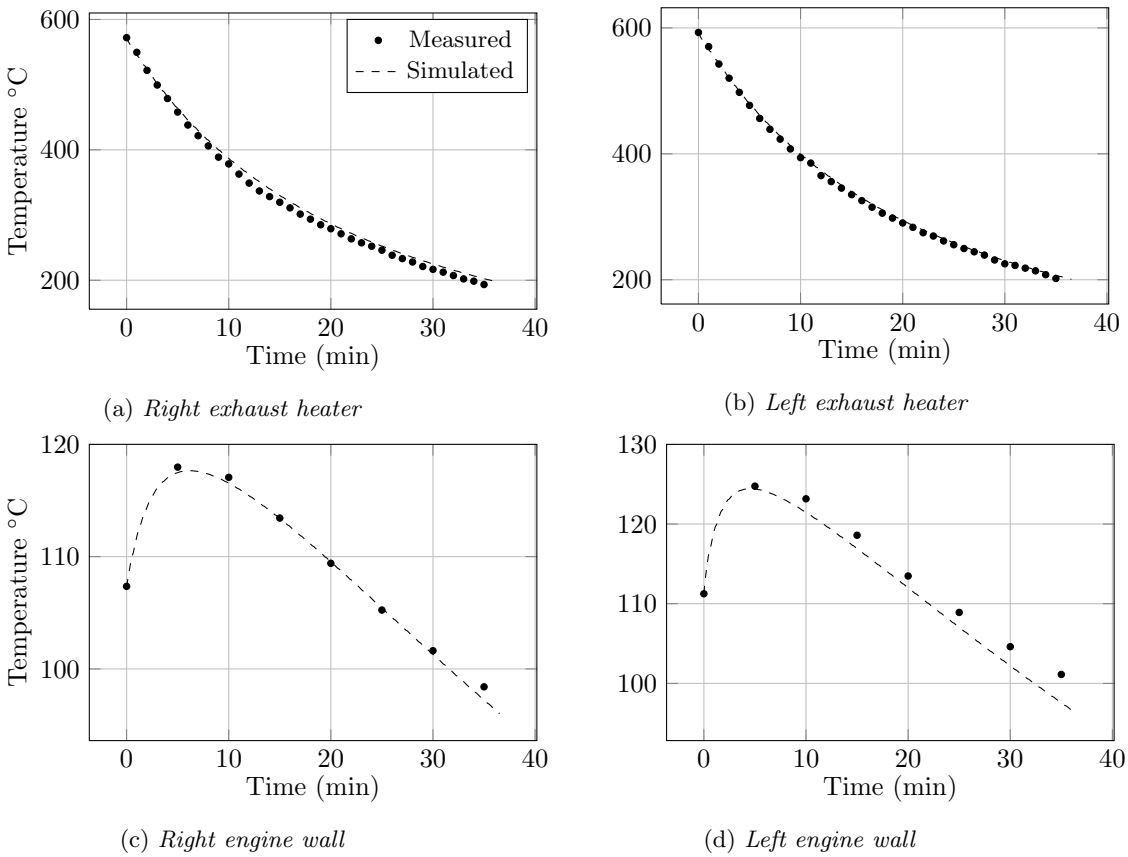


(a) *Right exhaust heater*

(b) *Left exhaust heater*

(c) *Right engine wall*

(d) *Left engine wall*

Figure 3.5: *Comparison between the computed and experimentally measured average surface temperatures of the engine solids during cool-down.*

simulated coolant flow rate through the radiator. Observed is an accurate correlation between the measured and the predicted values for the coolant mass flow rate through the radiator. A computation of the oil temperature variation during engine cool-down after a high-load driving is performed for validation purposes. Figure 3.7 presents a comparison between the simulated and the measured oil and coolant temperatures. The dynamic vehicle model combined with the mapped engine are active during the initial 1500 seconds of the simulation cycle, when they supply information for the instantaneous heat rate to the thermal engine representation. Upon key-off this signal becomes zero. After engine shutdown the variation in temperature of engine solids and fluids depends on the heat transfer rate from the respective engine surfaces to the ambient air, captured by the 3D CFD modules and synchronized with the 1D thermal engine representation.

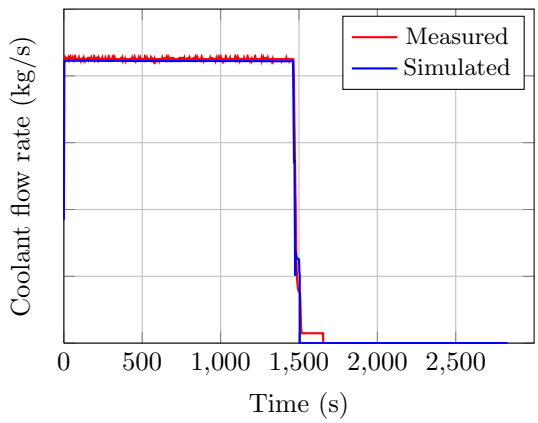


Figure 3.6: *Comparison between measured and simulated coolant flow rate through the radiator.*

Figure 3.7a presents a comparison between the predicted and the measured values for the coolant temperature in the engine block during high load driving and immediately after engine shutdown. Captured is the abrupt temperature drop after key-off due to a temporary fan engagement. This is followed by an increase and a peak in the coolant temperature as a result of the thermal soaking after fan disengagement. The discrepancy in the prediction for the coolant temperature is explained with the shortcomings of the 1D thermal engine model that fails to appropriately capture the physics of the low-Reynolds-number thermal phenomenon that occurs in the engine block in the absence of forced coolant flow. Furthermore, the measured values are affected by the exact placement of the temperature probe, which cannot be adequately replicated with the employed 1D setup of the thermal engine model. However, the obtained prediction for the coolant temperature correctly reflects the trend of variation. Figure 3.7b shows a close correlation between the measured and the simulated values for the oil temperature variation after key-off. The advantages of employing a detailed 3D representation of heat transfer in the oil sump are evident.

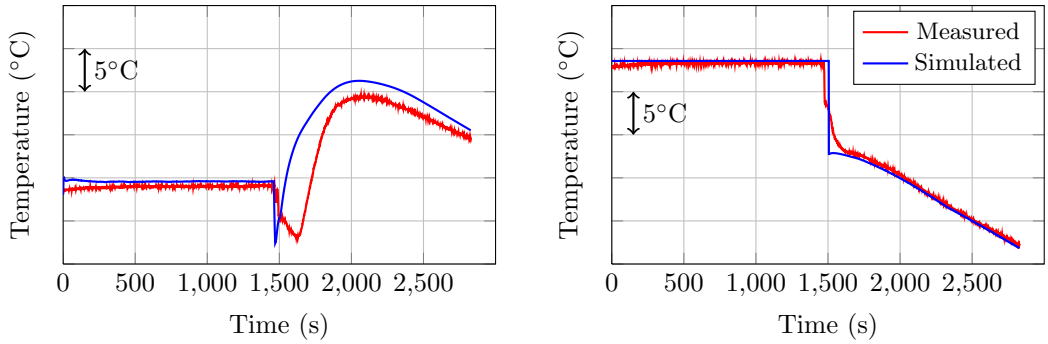


(a) *Coolant temperature in the engine block*

(b) *Temperature in the oil sump*

Figure 3.7: *Comparison between the measured and the simulated fluid temperatures in the powertrain cooling systems.*

## 3.3 Simulation of heavy-duty engine cool-down

The current section presents a similar validation of the computational method, however, now the comparisons between measured and simulated values for the temperatures of fluids and engine structures are performed over an extended time period for a commercial vehicle.

### 3.3.1 Experimental setup

The presented validation is based on temperature measurements obtained from thermocouples mounted on the surfaces of the cylinder head, block, crankcase, and gearbox of a Volvo FM distribution truck. The temperature readings are monitored for over nine hours after engine shutdown. The temperature of the oil in the sump is also measured during the cool-down period. The measurements were performed in a climatic windtunnel at an ambient temperature of 25°C at the absence of any forced flow. Figure 3.8 shows the locations of the thermocouple probes during the measurements.

### 3.3.2 Numerical setup

A 1D representation of heat transfer in the engine structures is set up by following the methodology described in section 2.1.4. The latter is coupled with a 3D CFD representation of the complete vehicle in the climatic wind tunnel. The previously described 1D–3D coupled procedure is applied to simulate the continuous variation of the temperatures of engine structures. The temperature variation in the engine oil is captured by a separate transient CFD model of the crankcase and the oil. This model is also coupled and synchronized with the 1D model of conduction in the engine structures.

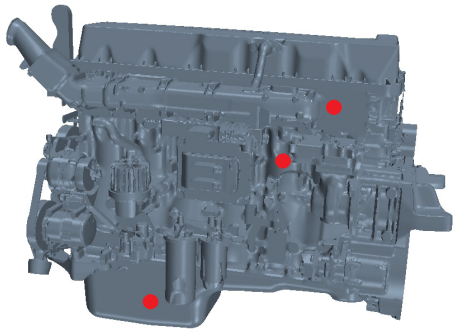

Figure 3.8: *Locations of the thermocouples for measuring the extended engine cool-down in a Volvo FM truck.*

### 3.3.3 Results

Presented below are comparisons between the measured and the computed variations in the temperature of the engine oil, the cylinder head, the engine block, and the crankcase at an ambient temperature of 25°C after the vehicle is turned off.

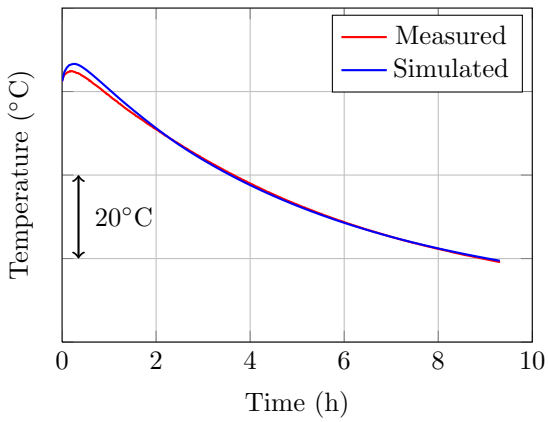


Figure 3.9: *Comparison between the measured and the simulated temperatures of the cylinder head after key-off at an ambient temperature of 25° C.*

Figure 3.9 presents a good agreement between the measured and the simulated temperatures of the cylinder head. The simulated temperature variation begins with a short-term increment, which corresponds with the measured values and occurs due to the sudden interruption of the cooling fluid streams, combined with the radiation and conduction heat transfer from the hot exhaust manifold and other components of the exhaust system. The physical properties of the thermal masses, used to represent the cylinder head in the 1D model, are obtained from available geometric data. The heat transfer and the flow in the oil sump are calculated from a separate transient CFD

representation, which is synchronized and coupled with the main simulation.

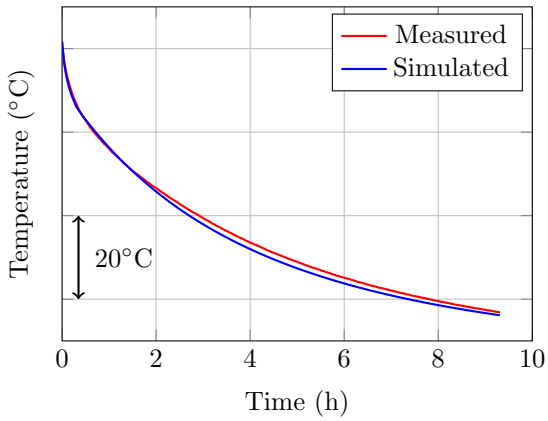


Figure 3.10: *Comparison between the measured and the simulated temperatures of the engine block after key-off, at an ambient temperature of 25° C.*

A good correlation between the simulated and the measured values is observed for the temperature of the engine block, Figure 3.10.

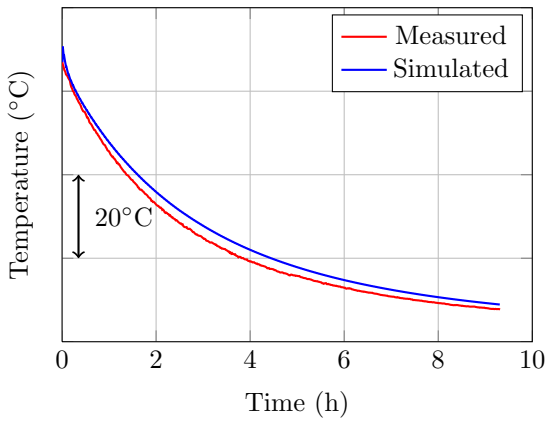


Figure 3.11: *Comparison between the measured and the simulated average temperature of the crankcase wall at an ambient temperature of 25° C.*

A minor discrepancy (of approximately 4°C) is observed in the prediction of the mean temperature of the crankcase wall. This may be a result of the the fact that in reality there is a considerable temperature difference across the surface of the crankcase, which results from the strong presence of temperature stratification in the contained oil. The plotted temperature is the surface-average boundary temperature, which differs from the local measurement taken by the surface-mounted probe.

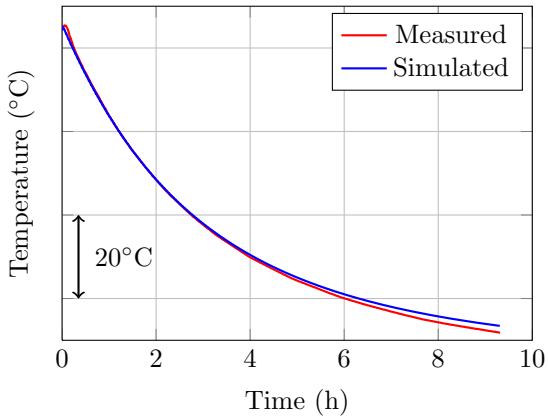


Figure 3.12: *Comparison between the measured and the simulated local temperatures of engine oil after key-off at an ambient temperature of 25° C.*

An overprediction of the oil temperature is observed towards the end of the simulated cool-down period on Figure 3.12. This is explained by a minor difference in the simulated total oil mass in the crankcase and the actual oil content in the physical test. Despite some minor inaccuracies, the simulated temperature variations of the engine structures and the oil are consistent with the measured values up to 9 hours after key-off.

## 3.4 Simulation of a combined drive-cycle with a period of engine inactivity

Presented next are the results from simulations of a sequence of two WLTC separated by different lengths of engine inactivity for a passenger vehicle, Volvo S80, with and without engine encapsulation at two different ambient temperatures. Furthermore, the encapsulated variants are simulated in two configurations: with closed shutters and with an open outlet shutter. This study demonstrates the full functionality of the combined model, that was developed by the author, for analyzing the effects of engine encapsulation on engine cool-down. Simulated readings for fuel consumption are also reported.

### 3.4.1 Numerical setup

A complete numerical representation of the vehicle featuring a 1D–3D representation of buoyancy-driven heat transfer in the engine bay is set up according to the method described in chapter 2.

### 3.4.2 Results

Figure 3.13 shows the variation in the temperature of the engine oil during a sequence of WLTC separated by 16 hours of inactivity, at ambient temperatures of 5°C and 20°C.

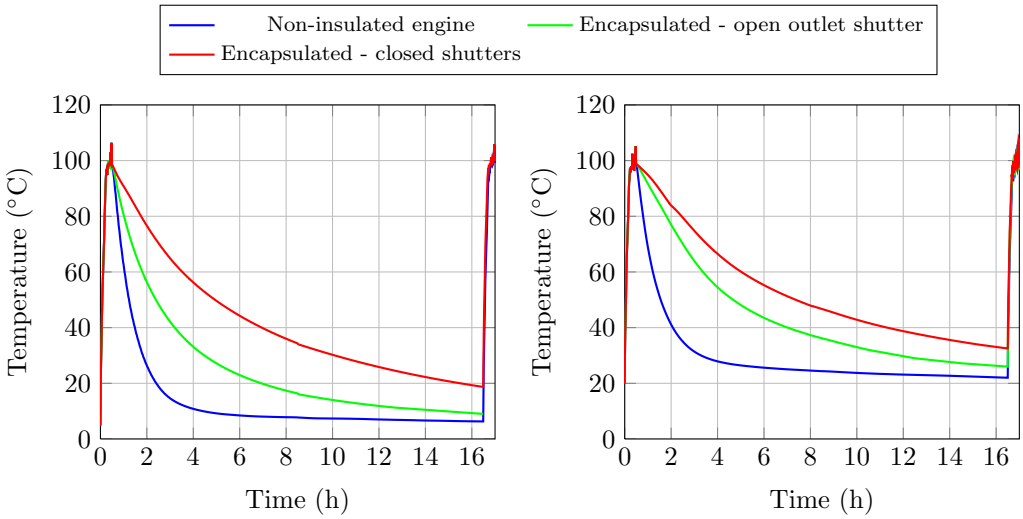


(a) *Ambient temperature 5° C* (b) *Ambient temperature 20° C*

Figure 3.13: *Variation in the engine oil temperature during a sequence of simulated WLTC with 16 hours of inactivity in a quiescent ambient.*

The temperature of the engine oil in the non-insulated engine decreases to ambient level within approximately 6 hours after key-off. On the other hand, the encapsulated configuration, with closed shutters, extends the cool-down time significantly, retaining the oil temperature to approximately 19°C 16 hours after engine shutdown at an ambient temperature of 5°C, and to 32°C at an ambient temperature of 20°C. The thermal engine encapsulation contributes to reduced friction losses during engine warm-up by retaining a higher initial temperature for engine start. Figure 3.14 shows the increase in the initial temperatures of the engine parts as a result of the thermal encapsulation at an ambient temperature of 5°C. The solid curves represent the temperature increase in the encapsulated setup with closed shutters and the dashed curves show results from the encapsulation with open outlet shutters. As a result of the thermal engine encapsulation, the temperatures of the engine oil, the cylinder head and the block 4 hours after engine shutdown are 51, 51 and 43°C higher than their corresponding levels in the non-encapsulated engine (at an ambient temperature of 5°C), respectively.

Figure 3.15 shows the variation in the engine oil temperature upon engine start after 4 hours of inactivity. The obvious effect from the higher initial temperature of the engine oil and structures is a faster engine warm-up. The encapsulated configuration with closed shutters achieves approximately 10 minutes faster warm-up compared to the non-insulated engine. The effects of this heat storage capability on the fuel consumption are presented in Figure 3.16 as a percentage of the total fuel burned by a cold-started non-encapsulated engine during the WLTC at ambient temperature of 5°C. The encapsulated engine with a closed outlet achieves a peak of 3.1% reduction of fuel consumption 3 hours after key-off. The potential for fuel saving gradually increases after engine shutdown in proportion with

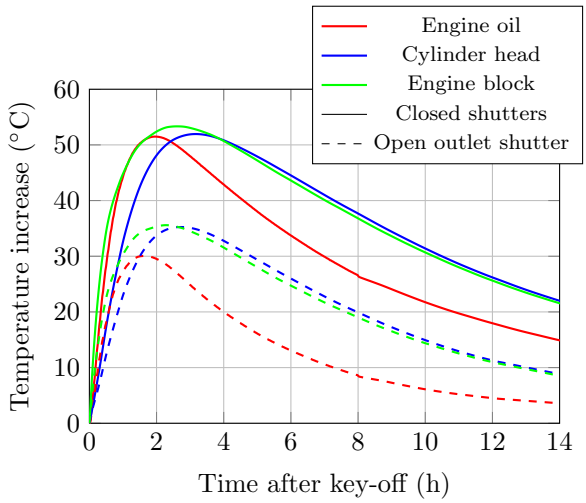


Figure 3.14: *Increase in the temperature of engine parts as a result of the encapsulation after key-off in a quiescent ambient of 5° C.*

the temperature increase in the engine components shown in Figure 3.14. The highest potential for fuel savings (larger than 2.5%) is yielded for applications where cold starts occur every 2 to 8 hours. The completely enclosed encapsulation delivers 2% fuel savings up to approximately 10 hours after key-off at 5°C ambient temperature.

Due to its superior insulating capability the closed encapsulation effectively retains engine heat within its boundaries. The low thermal conductivity of the insulating material minimizes conductive heat fluxes through the encapsulating wall. This is confirmed by only a minor increase of the air temperature in proximity to the external wall of the encapsulation with closed shutters in Figure 3.17. The minor temperature change along the vertical direction inside the encapsulation indicates little amount of mass transfer across its gaps. This is different in the case of open encapsulation, where the temperature field within the walls of the encapsulation varies in a wider span, see Figure 3.18. Cold air occupies the lower part of the encapsulation as a result of the increased mixing and mass transfer through the open shutter.

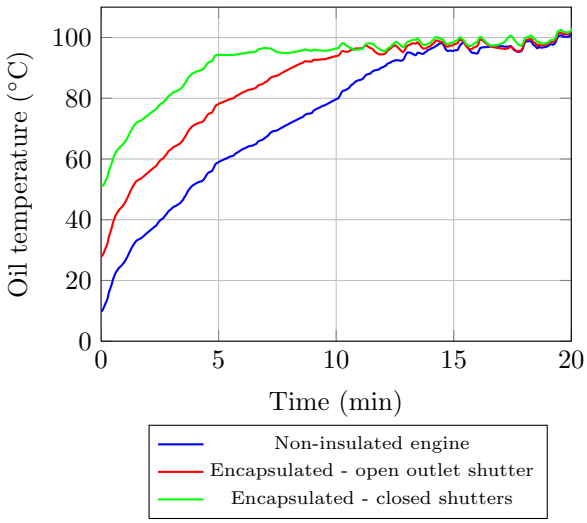


Figure 3.15: *Variation in the oil temperature after engine start preceded by 4 hours of inactivity at an ambient temperature of 5° C.*

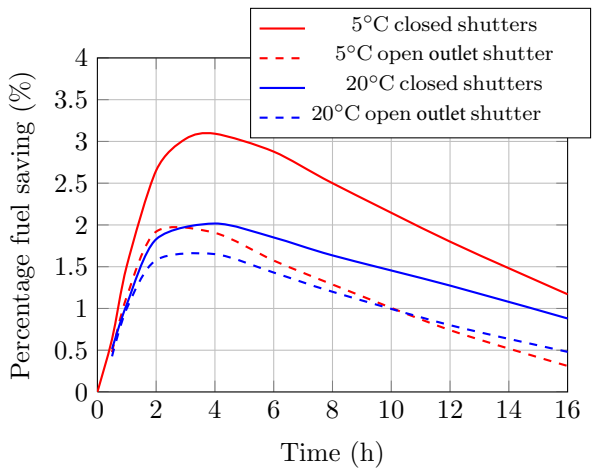


Figure 3.16: *Fuel savings expressed as percentage of the burned fuel by the non-encapsulated engine during WLTC at 5 and 20° C ambient temperature.*

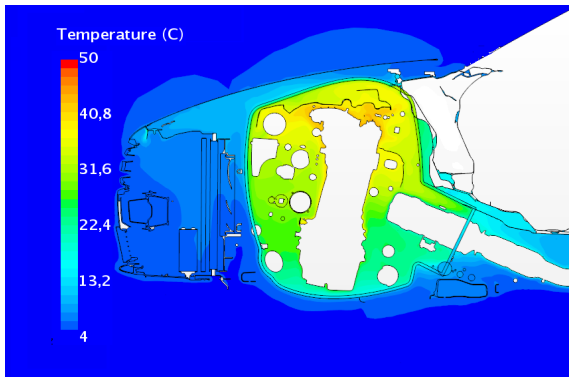


Figure 3.17: *The temperature field in the closed encapsulation approximately 10 hours after key-off, 5° C ambient temperature.*

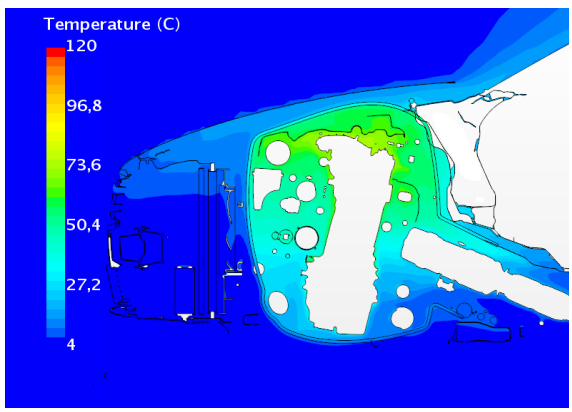


Figure 3.18: *The temperature field in the encapsulation with open outlet shutter approximately 2 hours after key-off, 5° C ambient temperature.*

# 4 Conclusions

The presented studies form a framework for numerically modeling the effects of thermal engine encapsulation on engine cool-down and fuel consumption during a continuous drive-cycle with engine stops. Thermal engine encapsulation can help reduce fuel consumption by retaining heat in the engine after it has been switched off. This slows engine cool-down and increases the chance for higher initial temperatures of the engine structures and fluids at the following engine start. Consequently, the friction losses in the cold-started encapsulated engine, which has retained heat from a previous engine start, would be lower during the shorter warm-up period, resulting in less fuel burned.

To obtain an analytical prediction for the fuel saving potential of a given encapsulation design, for a certain drive-cycle, the presented work utilizes a combined simulation platform. This consists of a complete 1D transient thermal representation of the powertrain and powertrain cooling systems coupled with a longitudinal vehicle dynamics model with drive-cycle input, a temperature-dependent engine friction model, and a coupled 1D-3D CFD model of engine cool-down after key-off. The 1D transient model of heat transfer in the engine and the powertrain cooling systems enables the prediction of temperatures of fluids and different engine components over the course of the entire drive-cycle. A coupled 1D-3D computational approach is used to predict the continuous variation of temperatures of the engine solids and fluids after engine shutdown. 3D CFD simulations compute the buoyancy-driven flow and heat transfer in the engine bay and oil sump after engine shut-down. In an iterative automated procedure, the heat transfer coefficients are updated in the 1D thermal representation of heat conduction in the engine solids. With the aid of a temperature-dependent engine friction model the energy savings due to decreased oil viscosity are accounted for and an instantaneous reading for fuel consumption is obtained.

The presented simulation strategy is applied to predict the fuel savings resulting from a proposed engine-mounted encapsulation designed for a passenger vehicle at different ambient temperatures. The results show that a fully-encapsulated engine is capable of retaining the temperature of engine oil at 19°C for up to 16 hours after engine shut-down in an ambient environment of 5°C. As a result of this heat-retaining capability of the encapsulated engine, it is possible to gain up to a 3.1% fuel saving from the total fuel burned during a WLTC with a cold-started engine. The results from simulations show that a minimum of 2.5% can be obtained for an encapsulated engine (with 97%degree of coverage) for engine starts occurring 2 to 8 hours after key-off at ambient temperature of 5°C.

The performed analysis shows that the degree of coverage is important for the heat-retaining capability of the encapsulation. The overall applicability and usefulness of thermal engine encapsulation for a certain vehicle application depends on the length of the time periods when the engine is inactive, i.e. the time from the moment when the vehicle is parked to the moment when the engine is re-started. The more frequently a vehicle is subjected to cold-starts during its lifetime, the higher the fuel-saving potential an encapsulation would have. The concept of thermal encapsulation of the powertrain is most beneficial in vehicle applications with short and frequent drive-cycles in cool climates.

# 5 Summary of papers

## 5.1 Paper A

"Study of Software Integration for Transient Simulation of Future Cooling System for Heavy Truck Application"

The first paper in this thesis considers transient simulations of the cooling system in a heavy-duty vehicle. The work investigates the integration between tools for analysis and simulation of cooling systems at Volvo Group Trucks Technology. The focus is on 1D simulation tools, which are generally preferred in the context of transient simulations of engine and powertrain installation systems. This work delivers two transient models of FH 13L cooling system integrated with a predictive model of the engine and a detailed model of the main coolant circuit. Also included is a representation of the underhood cooling air path. The simulation models deliver satisfactory level of accuracy for the predictions of the coolant temperature at different parts of the cooling system for the investigated drive-cycle. The computational speed of the model run on a single CPU is approximately 1×RT.

## 5.2 Paper B

"Numerical Investigation of Natural Convection in a Simplified Engine Bay"

This paper presents results from numerical investigations of buoyancy-driven flow in a simplified representation of an engine bay. A main motivation for this study is the necessity for a valid correlation of the results from numerical simulations with physical measurements in order to evaluate the accuracy and feasibility of the available numerical tools for predicting natural convection. This analysis is based on previously performed PIV and temperature measurements in a controlled physical setup, which reproduced thermal soak conditions in the engine compartment as they occur for a vehicle parked in a quiescent ambient after sustaining high thermal loads. Thermal soak is an important phenomenon in the engine bay primarily driven by natural convection and radiation after there had been a high power demand on the engine. With the cooling fan turned off and in quiescent environment, buoyancy driven convection and radiation are the dominating modes of heat transfer. The unsteady and turbulent nature of this complex phenomenon requires high spatial and temporal resolutions and an effective computational strategy. A CFD procedure for modeling buoyancy driven flow in vehicle underhood is demonstrated. The computed temperature and velocity of the air under the enclosure are compared with experimental data at a number of different locations in the control volume. The numerical results exhibit satisfactory consistency with the measured values.

## 5.3 Paper C

"Direct Coupled 1D-3D Approach for Simulations of Buoyancy-driven Heat Transfer in a Simplified Engine Bay"

The objective of this work is to present and validate a detailed numerical procedure for predicting buoyancy-driven heat transfer (BDHT) inside a simplified vehicle underhood during thermal soak and cool-down events. A direct coupled 1D–3D approach is employed to carry out transient 1D thermal analysis in the engine solids synchronized with sequences of steady-state 3D CFD simulations of the fluid flow. The boundary heat transfer coefficients and averaged fluid temperatures in the boundary cells, computed in the 3D CFD model, are provided as input data to the 1D analysis to compute the resulting surface temperatures which are then fed back as updated boundary conditions in the CFD simulation. The presented numerical procedure is validated using relevant experimental measurements. The computed temperatures of the simplified engine and the exhaust manifolds during the hot-soak and cool-down period are in favorable agreement with the experimental measurements. The present study illustrates the capabilities of the coupled thermal methodology to conduct accurate and cost-effective computations of BDHT for industrially relevant thermal management applications.

## 5.4 Paper D

"A Numerical Investigation of Thermal Engine Encapsulation Concept for a Passenger Vehicle and its Effect on Fuel Consumption"

Thermal engine encapsulation is an effective design choice to reduce engine friction in applications with frequent cold starts. In the present work, a coupled 1D–3D system-level approach is used to investigate the effects of a novel engine-mounted encapsulation concept featuring air shutters on the fuel consumption of a Volvo S80 passenger vehicle. Simulations are performed for sequences of the WLTC, which include different time intervals of engine inactivity when the car is parked in a quiescent ambient. The results show that the engine encapsulation with high area coverage (97%) can retain engine oil temperature above 19°C for up to 16 hours after engine shutdown at ambient temperature of 5°C leading to 2.5% fuel saving during engine warm-up when cold starts occur between 2 and 8 hours after key-off.

# References


[1] Minovski, B., Lofdahl, L., and Gullberg, P., "Numerical Investigation of Natural Convection in a Simplified Engine Bay," *SAE Technical Paper 2016-01-1683,* (2016). DOI: 10.4271/2016-01-1683.

[2] Wang, Z., Han, J., and Mukutmoni, D., "Numerical Simulation of Unsteady Natural Convection in a Simplified Engine Bay Enclosure under Soak Conditions," *SAE Technical Paper 2014-01-0651,* (2014). DOI: 10.4271/2014-01-0651.

[3] A. Bejan. *Convection Heat Transfer.* John Wiley & Sons Inc, New York, 1995.

[4] C. Adapco. StarCCM+ Manual, 9.02.005 edition (2014).

[5] A.Muscio and E.Mattarelli. Potential of Thermal Engine Encapsulation on Automotive Diesel Engines (2005). DOI: 2005-24-067.

[6] Blago Minovski. *Coupled simulations of cooling and engine systems for unsteady analysis of the benefits of thermal engine encapsulation.* Licentiate thesis, Chalmers University of Technology, 2015.

[7] Y. A. Cengel, R. H. Turner, and J. M. Cimbala. *Fundamentals of Thermal-Fluid Sciences.* McGraw Hill, 2008. ISBN: 978-007-126631-4.

[8] Chen, K., Johnson, J., Merati, P., and Davis, C., "Numerical Investigation of Buoyancy-Driven Flow in a Simplified Underhood with Open Enclosure," *SAE Int. J. Passeng. Cars - Mech. Syst. 6(2):805-816,* (2013). DOI: 10.4271/2013-01-0842.

[9] C. Davis. *Investigation of Underhood Buoyancy driven Flow and Thermal Measurements in a Simplified Full Scale Underhood Engine Compartment with Open Enclosure.* Master Thesis. Kalamazoo, Michigan: Western Michigan University, 2009.

[10] *EU $CO_2$ emission standards for passenger cars and light-commercial vehicles.* International Council on Clean Transportation, 2014.

[11] F. Fortunato et al. Underhood Cooling Simulation for Development of New Vehicles (2005). DOI: 2005-01-2046.

[12] *GT-SUITE Flow Theory Manual Version 7.5.* Gamma Technologies. 2014.

[13] J. B. Heywood. *Internal Combustion Engine Fundamentals.* McGraw Hill International Editions, 1988.

[14] K. Holmberg and P. Andersson. Global energy consumption due to friction in trucks and busses. *Tribology International* (2014).

[15] W. H. Hucho. *Aerodynamics of road vehicles.* Society of Automotive Engineers, 1998.

[16] I. V. Miroshnichenko and M. A. Sheremet and A. A. Mohamad, Numerical simulation of a conjugate turbulent natural convection combined with surface thermal radiation in an enclosure with a heat source. *Int. J. Therm. Sci.* **109** (2016), 172–181.

[17] S. Kaushik. Thermal Management of a Vehicle's Underhood and Underbody Using Appropriate Math-Based Analytical Tools and Methodologies (2007). DOI: 2007-01-1395.

[18] Lauriat, G. and Desrayaud, G., Effect of surface radiation on conjugate natural convection in partially open enclosures. *Int. J. Therm. Sci.* **45** (2012), 335–346.

[19] Leong, D. K. W., Shayler, P.J.,Pegg, I.G., Murphy, M. Characterising the effect of viscosity on friction in the piston assembly of internal combustion engines. *Journal of Engineering Tribology* **221**.4 (2007), 469–478.

[20] M. F. Modest. *Radiative Heat Transfer, Series in Mechanical Engineering*. McGraw-Hill.

[21] K. Mahmoud, E. Loibner, and J. Krammer. Integrated 1-D Tools for Modeling Vehicle Thermal Management System (2004). DOI: 2004-01-3406.

[22] D. M. Mantovani et al. Innovative concepts for thermo-acoustic engine compartment encapsulation (2010). URL: www.rieter.com.

[23] P. Merati et al. Underhood Buoyancy Driven Flow - An Experimental Study. *J. Heat Transf.* **133** (2011), 082502 (1–9).

[24] B. Minovski and L. Löfdahl. Study of Software Integration for Transient Simulation of Future Cooling System for Heavy Truck Application (2014). DOI: 10.4271/2014-01-0653.

[25] B. Minovski, L. Löfdahl, and P. Gullberg. A 1D Method for Transient Simulations of Cooling Systems with Non-Uniform Temperature and Flow Boundaries extracted from a 3D CFD solution (2015).

[26] Minovski, B. and Lofdahl, L., "Study of Software Integration for Transient Simulation of Future Cooling System for Heavy Truck Application," *SAE Technical Paper 2014-01-0653,* (2014). DOI: 10.4271/2014-01-0653.

[27] Mustafa, R., Schulze, M., Eilts, M. Improved Energy Management Using Engine Compartment Encapsulation and Grille Shutter Control. *J. Fuels Lubr* **5**.2 (2012). DOI: 2012-01-1203.

[28] B. Petroleum. BP Statistical Review of World Energy June 2014 (2014). URL: http://www.bp.com/statisticalreview.

[29] R. De Césaro Oliveski, M. H. Macagnan, J. B. Copetti, A. de La Martinière Petroll. Natural convection in a tank of oil: experimental validation of a numerical code with prescribed boundary condition. *Experimental Thermal and Fluid Science* **29** (2005), 671–680.

[30] Redrawing the energy-climate map. *OECD/IEA International Energy Agency* (2013).

[31] A. Roberts, R. Brooks, and P. Shipway. Internal combustion engine cold-start efficiency: A review of the problem, causes and potential solutions. *Journal of Energy Conversion and Management* **82** (2014).

[32] B. Rosenau. Multifunctional Encapsulations of the Power Train (2003).

[33] R.Siegel. *Thermal radiation heat transfer*. Hemisphere Pub. Corp.

[34] Shayler, P.J., Allen, A.J., Leong, D.K.W., Pegg I., Brown A.J., Dumenil, J-C. Characterising lubricating oil viscosity to describe effects on engine friction. (2007). DOI: 2007-01-1984.

[35] F. Storkenmaier, M. Brinkammer, and V.Caldiero. Multifunctional Encapsulations of the Power Train (2006). DOI: 2006-01-1234.

[36] Storkenmaier, F., Birnkammer, M., Caldiero, V., Manschitz, M. et al., "Multifunctional Encapsulations of the Power Train," *SAE Technical Paper 2006-01-1234,* (2006). DOI: 10.4271/2006-01-1234.

[37] Sweetman, B., Schmitz, I., Hupertz, B., Shaw, N. et al., "Experimental and Numerical Investigation of Vehicle Drive and Thermal Soak Conditions in a Simplified Engine Bay," *SAE Int. J. Passeng. Cars - Mech. Syst. 10(2):433-445,* (2017). DOI: 10.4271/2017-01-0147.

[38] B. T. $CO_2$ and emission reduction by means of heat storage in the powertrain (2011). DOI: C1305/042/2011.

[39] H. K. Versteeg and W. Malalasekera. *An Introduction to Computational Fluid Dynamics*. Prentice Hall, 2007. ISBN: 978-0-13-127498-3.

[40] Zammit JP, Shayer PJ, Pegg I. Thermal coupling and energy flows between coolant, engine structure and lubricating oil during engine warm-up (2010).